European Journal of Chemistry 1 (2) (2010) 142-161

European Journal of Chemistry

Journal homepage: www.eurjchem.com

Theory and computations of two-photon absorbing photochromic chromophores

Artëm E. Masunov[a,b,c,d,*] and Ivan A. Mikhailov[a]

[a] *NanoScience Technology Center, University of Central Florida, Orlando, FL 32826, USA*
[b] *Department of Chemistry, University of Central Florida, Orlando, FL 32816, USA*
[c] *Department of Physics, University of Central Florida, Orlando, FL 32816, USA*
[d] *Florida Solar Energy Center, University of Central Florida, Cocoa, FL 32922, USA*

**Corresponding author at: NanoScience Technology Center, University of Central Florida, Orlando, FL 32826, USA. Tel.: +1.321.6622724; fax: +1.407.8822819.*
E-mail address: amasunov@gmail.com (A.E. Masunov).

REVIEW INFORMATION

Received: 11 March 2010
Received in revised form: 20 May 2010
Accepted: 23 May 2010
Online: 30 June 2010

KEYWORDS

TDDFT
Organic photochemistry
Photocyclization
Photoinduced reactions
Two-photon absorption
State-to-state transition dipoles

ABSTRACT

Exponential growth in information technology generates ever increasing amounts of data, making recording density of the storage media crucially important. Two-photon absorption was proposed as a basis for high-density multi-layer technology for optical memory and logic devices. This technology suggests to use polymers, doped with photochromic compounds that undergo a reversible photoinduced isomerization, or photoswitching. In this review we consider recent theoretical works and benchmarking studies of the DFT-based methods, capable to predict two-photon absorption (2PA) and photochemical activity, Next we review the applications of these methods to design a prototype molecule that combines the photon-mode recording property of photochromic compounds with large 2PA cross-section. We conclude that a *posteriori* Tamm-Dancoff approximation to the second order CEO approach in Density Functional Theory is the powerful tool for both quantitative predictions and qualitative understanding of the excited state processes in photophysics and photochemistry. We also emphasize general principles for the rational design of a two-photon operated photoswitch.

1. Introduction

Exponential growth in the information technology industry generates ever increasing amounts of data. This made the recording density of storage media crucially important, and prompted development of optical solutions as an alternative to the traditional magnetic storage devices. Optical data storage refers to systems that use laser light for recording information as well as for readout. Most optical memory systems available on the market currently utilize inorganic materials and are based on magneto-optical [1,2] and phase-change [3] effects. Both effects are utilized in the heat-mode recording, where the light energy is converted into heat. This induces a magnetic or structural phase transition, and changes physical properties of the medium.

Until recently, organic materials have not been considered as viable candidates because of insufficient reliability. However, the situation has changed after CD-R (compact disk-recordable) technology was introduced. This technology is based on organic dyes as the memory medium, and uses polymers, doped with photochromophores (the molecules, which undergo a reversible photoinduced isomerization or photochromism) [4]. Photochromism is a non-destructive process involving a light initiated rearrangement of chemical bonds accompanied by change in color and other properties. An example of photochromophores is diarylethene compounds, shown on Scheme 1. They undergo photochromic processes, involving the photoinduced conrotatory opening and closing of the central bond, and fulfill requirements needed for material applications, namely, thermal stability and resistance to linear optical photofatigue [5].

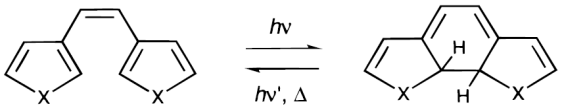

Scheme 1. Diarylethene photoswitching X = O or X=S. hν stands for photon absorption, Δ – thermal process.

Photon-mode data recording is expected to win the competition with magnetic and heat-mode optical recording. Photochromic materials are now considered to be promising candidates for erasable memory media of the next generation. Another important property of photochromic materials is an ultrafast change of the state upon irradiation. Photochromic compounds with ultrafast switching capabilities can be also useful for optical communication, signal processing, and interconnection as components of various photonic devices, such as optical switches, variable frequency filters, attenuators, and phase shifters.

Besides reversibility and ultrafast switching, photochromic optical data storage devices (as opposed to heat-mode ones) possess another important advantage. They offer a possibility of data recording using individually addressable 3-dimensional arrays of bits. Three-dimensional design opens an opportunity of using hundreds of layers beneath the optical disk surface, thus increasing storage capacity two orders of magnitude and more. In order to increase a storage density one needs to

ISSN 2153-2249 (Print) / ISSN 2153-2257 (Online)
DOI:10.5155/eurjchem.1.2.142-161.119

reduce the parasite cross-talk between these recorded layers; to this end Rentzepis *et al.* suggested using two-photon absorption of light [6].

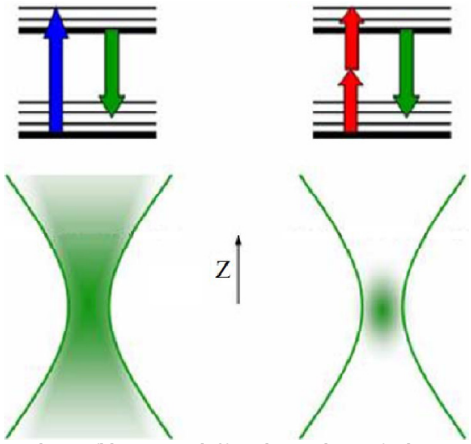

Figure 1. One-photon (blue arrow, left) and two-photon (red arrow, right) initiated transitions between molecular energy levels. Z defines direction of the laser beam. Regions that are appreciably excited are shown in green. 2PA-related processes are more localized in space.

Two-photon absorption (2PA) is a nonlinear optical process in which chromophores, that would normally be excited by a single photon (1PA) of ultraviolet light are excited by two photons of near-infrared wavelengths (Figure 1). The probability of 2PA is quadratically dependent on intensity of the incident radiation, which opens a possibility of spatial localization. A longer wavelength provides a better penetration in absorbing or scattering media, and the quadratic dependence of the absorption probability on the light intensity allows for high 3D spatial selectivity through the use of a tightly focused laser beam. Under tight focusing conditions, the absorption is confined at the focus to a volume of order λ^3 (where λ is the laser wavelength), and any subsequent process, such as fluorescence or photoinduced chemical reactions, is localized in this small volume.

A number of molecular structures were designed as candidates for 2PA initiated photochromic materials [7], but were found to have insufficient 2PA cross-sections. A functioning 2PA based 3D optical storage system was reported recently [8]. It offered an interlayer separation of 5 μm and depth of up to 600 μm. However, the diode laser commonly used in DVD devices was not able to provide sufficient intensity to record information, and a higher-power solid-state laser was used for recording. Thus, design of photochromic dyes with higher 2PA cross-sections and quantum yields is vitally important for practical applications. The engineering of such materials is in need of rational strategies able to guide the progress in the material design.

There are two aspects of this rational strategy: prediction of the two-photon absorption cross-sections of a candidate, and prediction of its photochemical reactivity. These aspects are described in the following Subsections 2 and 3. Each of them includes a theoretical background, benchmark study and relevant applications. The final Subsection suggests a combination of methods for the rational design of a 2PA initiated photochromic switch.

Computational photochemistry offers a number of theoretical methods for investigation of photochemical reaction mechanisms. Unlike thermally activated chemical reactions, which take place in the ground electronic state (S_0), a photochemical process involves the electronically excited state (S_1). During this process the reactive system is electronically excited from S_0 to S_1, and after some evolution on the upper potential energy surface (PES) decays back to the ground state in either product or reactant basin through conical intersections (CIX) [9].

While accurate quantum dynamics calculations [10-12] for triatomic systems with CIX have been performed, large molecules of practical interest, necessitate the semi-classical [12,13] approach. In this approach adiabatic surfaces are treated classically, while transitions between them estimated using quantum mechanics. Another approximation involves reducing dimensionality of the system to two degrees of freedom and treating the resulting two-dimensional problem using wave packets [14]. Further simplification is called Pathway Approach [15]. Instead of entire PES, it considers a minimum energy path [16], which is followed by the center of the wavepacket [17]. This approach is focused on local properties of the PES, such as minima, barriers, and slopes. In this Pathway approach, CIX serves as a funnel, which delivers the excited state intermediate to the ground state reactant or the product, so that quantum yield is largely determined there [18]. It has been found very useful for qualitative analysis of the reaction mechanisms, prediction of photoproducts, and rationalization of experimental excited state lifetimes, quantum yields, absorption and emission spectra [19,20].

A number of computational tools have been developed to predict the PES [18,21,22]. Most of them are based on the Complete Active Space (CAS) method, where molecular orbitals are determined self-consistently within a multiconfigurational ansatz (full configuration interactions in a limited orbital space). While this method yields acceptable molecular geometries, the account for dynamic electron correlation is required for accurate energy predictions, and is typically accomplished by the multireference configuration interaction or perturbation theory treatment. These methods are computationally expensive and impractical for PES exploration in large molecular systems.

Formalisms based on density functional theory (DFT) are being considered among the more affordable alternatives. One of the approaches to treat excited states with DFT is the delta-Self Consistent Field (ΔSCF), where one of the occupied spin-orbitals is replaced with one of the unoccupied spin-orbitals in the Kohn-Sham determinant, and orbital relaxation with the SCF procedure is repeated. In general, such Kohn-Sham determinant with Fermi hole presents a saddle point and special orbital optimization algorithms are required [23]. In practice, ΔSCF is possible if the switched orbitals belong to different irreducible representations. This limitation is avoided in the restricted open-shell Kohn-Sham (ROKS) method [24], which is based on the Ziegler sum rule [25], stating that a single Kohn-Sham determinant with two orbitals occupied by unpaired electrons of the opposite spin is a 50/50 mixture of pure singlet and triplet states and therefore has energy which is an average between the two. This method was shown capable to describe geometry and perform molecular dynamics of the open shell singlet excited state, calculate the non-adiabatic coupling [26], and include the S_0–S_1 surface hopping into molecular dynamics simulations [27]. However, the double excited state, describing the photoreactive system in pericyclic minimum is not available in the ROKS methods.

An alternative approach to study PES of electronically excited systems is based on the time-dependent (TD) or, more precisely, linear response DFT formalism. Instead of orbital relaxation, TD-DFT uses an alternative procedure where the Kohn-Sham (KS) wavefunction is expanded in terms of Slater determinants, singly excited with respect to the reference state. A rigorous formulation of TD-DFT [28] demonstrates that this description is in principle exact, given that the frequency-dependent exchange-correlation functional is known. In most practical applications, however, this frequency dependence is ignored (so called adiabatic TD-DFT). This method was often reported to accurately predict electronic spectra and excited

state geometries. However, TD-DFT was found to be somewhat less successful in description of PESs in the vicinity of a CIX [29]. The recent study [30] demonstrated that these difficulties may be routed in the failure of the restricted Kohn-Sham formalism for the reference ground state close to the geometry of the pericyclic minimum, and introduced a possible solution, reviewed below in Section 3.

2. Prediction of two-photon absorption cross-sections

2.1. TD-DFT and a posteriori Tamm-Dancoff approximation to the second-order TD-DFT

Density functional theory in the KS approximation [31] was a method of choice in the solid state theory for a long time. It received recognition as a reasonably accurate first principles method for the ground states of large molecular systems after the Generalized Gradient approximation was combined with a fraction of Hartree-Fock (HF) exchange (hybrid GGA) [32]. Instead of a multiconfigurational wavefunction, the KS method accounts for electron correlation through the exchange-correlation potential. In particular, contributions of the double and higher excited configurations to the ground states are included in the single Slater determinant KS description implicitly. It was shown that the exact electron density obtained in multireference *ab initio* methods (such as Full Configuration Interaction) can be mapped onto an effective single-particle KS description even for molecules far from the equilibrium [33]. The ground state wavefunction is simply not available in DFT for analysis, and the single KS determinant describes hypothetical system of noninteracting electrons used in the KS theory, rather than a molecular system of interest. Despite the single determinant appearance, DFT is not a single reference method. This statement becomes apparent when the Fermi broadening is applied to the occupation numbers, and these fractionally occupied KS orbitals are compared with Natural orbitals, obtained in one of wavefunction based methods [34]. From a practical standpoint, approximate hybrid exchange-correlation functionals (such as B3LYP [35]) result in energies close to coupled cluster models in quality [32]. There are several extensions of DFT, developed to describe the excited states. One approach is to use multireference strategies [36-39]. More often, however, DFT is combined with the time dependent perturbation theory approach, which we shall briefly review next.

Instead of obtaining lowest energy solutions to the Schrödinger equation based on the variational principle, excited states can be described by the time-dependent perturbation theory treatment as interaction between the molecular system and the electric field [40]. Several formalisms had been developed to obtain excitation energies and transition dipoles directly [41], including the equation of motion (EOM) and polarization propagator approaches. When the terms of second and higher order in the external filed are neglected (linear response, LR), and the HF method is adopted for description of the ground state, the approach is called Time-Dependent Hartree-Fock (TDHF) method, also known as random phase approximation (RPA). When applied to DFT ground state [28,42], the LR approximation is often called LR-DFT, or TD-DFT. The LR-DFT method results in non-Hermitian eigenvalue problem:

$$\begin{pmatrix} A & B \\ -B & -A \end{pmatrix}\begin{bmatrix} X \\ Y \end{bmatrix} = \Omega\begin{bmatrix} X \\ Y \end{bmatrix} \qquad (1)$$

solution to which are the excitation energies Ω_α and transition density matrices ξ_α for the ground to excited state transitions. In the basis of occupied (i,j) and vacant (a,b) KS orbitals of σ,τ subsets (σ,τ=α,β), transition density is block-diagonal with occupied-vacant $X = (\xi)_{ia}$ and vacant-occupied $Y = (\xi)_{ai}$ blocks being nonzero. Matrices ***A*** and ***B*** are defined as

$$A_{ai\sigma,bj\tau} = \delta_{ab}\delta_{ij}\delta_{\sigma\tau}(\varepsilon_a - \varepsilon_i) + K_{ai\sigma,bj\tau}$$

and

$$B_{ai\sigma,bj\tau} = K_{ai\sigma,jb\tau} \qquad (2)$$

For the hybrid DFT with c_{HF} fraction of the HF exchange, the coupling matrix ***K*** is expressed through the second derivatives of the exchange-correlation functional *w*, Coulomb and exchange integrals as:

$$K_{ai\sigma,bj\tau} = (1 - c_{HF})(ia \mid w \mid jb) + (ia \mid jb) - c_{HF}\delta_{\sigma\tau}(ab \mid ij) \qquad (3)$$

The RPA, or TDHF, equation is then a limiting case with c_{HF}=1, where the matrix ***A*** consists of interactions between two singly-excited configurations $(a \leftarrow i \mid H \mid b \leftarrow j)$, also known as the configuration interaction limited to singles (CIS) Hamiltonian. The matrix ***B*** includes, by virtue of swapping indexes, the excitations from virtual to occupied molecular orbitals (deexcitations) of the form $(a \leftarrow i \mid H \mid j \leftarrow b)$. Mathematically, they are equivalent to the matrix elements between the ground and doubly excited states [43]. Thus, LR-DFT accounts for double excitations in two ways: implicitly, though the exchange-correlation functional, and explicitly, through the deexcitation matrix ***B***.

Sometimes an additional approximation is introduced in the LR formalism. It is called Tamm-Dancoff approximation (TDA) [44,45], and consists in neglecting the deexcitation matrix ***B*** in equation (1). When applied to the HF ground state, it is equivalent to the CIS method. Double excitation character is included in the TDA-DFT formalism only implicitly through the approximate exchange-correlation (XC) potential. TDA was found to be accurate when an exact XC potential was restored from an exact electron density in systems close to equilibrium [46] (but not when covalent bond is stretched [47]). To a certain extent, TDA may correct the deficiencies in the approximate exchange-correlation functionals [48].

In practice, an implicit account for double excitations was found to be more important than the role of the deexcitation matrix. For instance, the study of excited states in radicals [49], demonstrated that TD-DFT gives results comparable to TD-HF for single excited states and more accurate excitation energies for the double excited states. The results for linear polyenes were mixed. Several studies [48,50,51] had reported a correct state ordering only with pure XC functionals (and not with more accurate, otherwise hybrid, functionals), combined with Tamm-Dancoff approximation and diffuse basis functions. Both successes and failures of LR-DFT to describe potential energy surfaces of single and double excited states, conical intersections between states, and photochemical transformations have been reported [29,52,53].

The alternative approaches, taking one lowest double-excited states into account explicitly at the LR level had been recently developed. Spin-flip DFT [54], and noncollinear XC with spin-flip excitations [55] use the $(HOMO)^1(LUMO)^1$ triplet (where HOMO and LUMO stand for the highest occupied and lowest unoccupied molecular orbitals respectively) as a reference state and obtain both the ground and double excited states as single excitations. Another approach, called Dressed TD-DFT [56] introduces frequency dependence into the XC kernel (non-adiabatic approximation to TD-DFT) by means of adding matrix elements involving double excited $HOMO^2 \rightarrow LUMO^2$ configurations into matrices ***A*** and ***B*** of eq. (1). As a

result, the $2A_g$ state acquires the double excited character, and its energy is considerably lowered. Although double excitations could be included in extended or higher-order RPA formalisms [57], these methods did not receive wide attention. Instead, LR has been applied to correlated ground states, including Multi-Configuration Self Consistent Field (MCSCF) [58], and Coupled Cluster (CC) [59-61] methods.

Let us focus on the transition dipole moments next. In LR-DFT they are readily obtained as convolution of the dipole moment operator with the transition densities:

$$\mu_\alpha = Tr(\mu\xi_\alpha) \tag{4}$$

State-to-state transition dipoles $\boldsymbol{\mu_{\alpha,\beta}}$ do not appear in the LR approximation, unless the excited state α is taken as the reference state. In order to obtain the expressions for $\boldsymbol{\mu_{\alpha,\beta}}$ one has to extend time dependent perturbation theory to Quadratic Response (QR). This extension was initially developed [62,63] for HF and MCSCF reference states using an explicit exponential unitary time dependent transformation. The results of the perturbation treatment were expressed in terms of response functions (first, second, and third-order corrections to the expectation values of an arbitrary operator). Many molecular properties may be extracted from single and double residues of these response functions [64] at the resonant frequencies (poles of the response function). Specifically, a transition dipole between excited states can be expressed through the ground state dipole moment $\boldsymbol{\mu_{o,o}}$, ground-to excited state dipole moments $\boldsymbol{\mu_\alpha}$ and $\boldsymbol{\mu_\beta}$, and the second residue of the dipole quadratic response function with two electric dipole perturbations $\boldsymbol{\mu^b}$ and $\boldsymbol{\mu^c}$ [63]:

$$\mu^a_{\alpha,\beta} = \mu^a_{0,0}\delta_{\alpha\alpha} - (\mu^b_\alpha\mu^c_\beta)^{-1} \lim_{\omega_b\to-\omega_\alpha}\left[\lim_{\omega_c\to\omega_\beta}(\omega_c-\omega_\beta)\left\langle\!\left\langle \mu^a;\mu^b,\mu^c\right\rangle\!\right\rangle\right](\omega_b-\omega_\alpha) \tag{5}$$

Substitution of the LR values in place of dipoles evaluated with the exact states leads to summation over large number of states. The explicit summation can be replaced by iterative solution of the linear equations [63], which may be recast [65] in a form, similar to eq. (1). Luo *et al.* studied linear polyenes (butadiene, hexatriene, and octatetraene) at the QR-HF level [66]. They found that the $1B_u$ state dominates the linear spectra, while three or four A_g states (depending on the basis set), that have large transition dipoles from the $1B_u$ state, appear on the two-photon absorption spectra with maxima near 1.5–1.7 of the bandgap (excitation energy of the $1B_u$ state). The quadratic response theory combined with DFT was also used for simulations of two-photon absorption spectra [67]. The quadratic response formalism, extended to CC [68] and DFT [69-71] reference states is implemented in the Dalton program [72].

An alternative formulation of time-dependent perturbation theory for excited states is known as Coupled Electronic Oscillator (CEO) approach [73,74]. It uses density matrix (Liouville space) representation and is based on the classical Heisenberg equation of motion for the ground state density. It was recently extended from the HF to DFT reference state [75]. When only terms of the first order in the external field are retained, equation (1), equivalent to the LR formalism is obtained. In the second order approximation, the solutions are sought in the basis of LR solutions (transition densities). As a result, linear excitations remain unchanged in the quadratic formalism, and combined states $\boldsymbol{\xi_\beta\xi_\alpha}$ of a double excited nature are added to the picture. The excitation energy for each of these new states is equal to the sum of single excitations:

$$\Omega_{\alpha\beta} = \Omega_\alpha + \Omega_\beta . \tag{6}$$

The second order CEO gives the transition dipole between the ground and this double excited state as

$$\mu_{0,\alpha\beta} = \sum_{\alpha\beta}^{perm} Tr(\mu(I-2\rho)\xi_\alpha\xi_\beta) + \sum_{\gamma>0}\left(\frac{V_{\alpha\beta-\gamma}\mu_\gamma}{\Omega_\alpha+\Omega_\beta-\Omega_\gamma} - \frac{V_{\alpha\beta\gamma}\mu_{-\gamma}}{\Omega_\alpha+\Omega_\beta+\Omega_\gamma}\right) \tag{7}$$

Here the first summation runs over symmetrized permutations of the indexes, second summation includes negative indexes, I is the identity matrix, ρ is the ground state density matrix, and $\boldsymbol{V_{\alpha\beta\text{-}\gamma}}$ is the exchange-correlation coupling term, expressed via KS operators $V(\xi)$ on transition densities:

$$V_{\alpha\beta-\gamma} = \frac{1}{2}\sum_{\alpha\beta\gamma}^{perm} Tr((I-2\rho)\xi_\alpha\xi_\beta V(\xi_\gamma)) \tag{8}$$

Further, the transition dipole between the double excited state and any other excited state is zero unless the other state presents one of the components of this double excited state:

$$\mu_{\alpha,\alpha\beta} = \mu_\beta ; \quad \mu_{\alpha,\beta\gamma} = 0 \tag{9}$$

The transition dipole between two single excited states is

$$\mu_{\alpha,\beta} = \sum_{-\alpha,\beta}^{perm} Tr(\mu(I-2\rho)\xi^*_\alpha\xi_\beta) + \sum_{\gamma>0}\left(\frac{V_{-\alpha\beta-\gamma}\mu_\gamma}{-\Omega_\alpha+\Omega_\beta-\Omega_\gamma} + \frac{V_{\alpha-\beta-\gamma}\mu_{-\gamma}}{\Omega_\alpha-\Omega_\beta-\Omega_\gamma}\right) \tag{10}$$

Thus, in the second order CEO the first double excited state of the $(HOMO)^2\rightarrow(LUMO)^2$ type is always twice higher in energy than the HOMO→LUMO excited state and (unlike in wavefunction based methods), it never mixes with single excitations. The perturbative treatment can be further extended to the third order, which results in corrections to the states and leads to the mixing of single, double and triple excitations within TD-DFT formalism (eq. G5-G7 in Ref. [75]):

$$\phi^{(0)} = |g\rangle_0 - \frac{1}{3!}\sum_{\alpha\beta\gamma>0}\frac{V_{-\alpha-\beta-\gamma}}{\Omega_\alpha+\Omega_\beta+\Omega_\gamma}a^\dagger_\alpha a^\dagger_\beta a^\dagger_\gamma|g\rangle_0, \tag{11}$$

$$\phi^{(1)}_\alpha = a^\dagger_\alpha|g\rangle_0 + \frac{1}{2!}\sum_{\beta\gamma>0}\frac{V_{\alpha-\beta-\gamma}}{\Omega_\alpha-\Omega_\beta-\Omega_\gamma}a^\dagger_\beta a^\dagger_\gamma|g\rangle_0, \tag{12}$$

$$\begin{aligned}\phi^{(2)}_{\beta\gamma} = {} & a^\dagger_\beta a^\dagger_\gamma|g\rangle_0 + \frac{1}{2!}\sum_{\alpha>0}\frac{2V_{-\alpha\beta\gamma}}{-\Omega_\alpha+\Omega_\beta+\Omega_\gamma}a^\dagger_\alpha|g\rangle_0 \\ & + \frac{1}{2!}\sum_{\delta\zeta>0}\left(\frac{V_{\gamma-\delta-\zeta}}{\Omega_\gamma-\Omega_\delta-\Omega_\zeta}a^\dagger_\beta + \frac{V_{\beta-\delta-\zeta}}{\Omega_\beta-\Omega_\delta-\Omega_\zeta}a^\dagger_\gamma\right)a^\dagger_\delta a^\dagger_\zeta|g\rangle_0,\end{aligned} \tag{13}$$

where $|g\rangle_0$, $a^\dagger_\alpha|g\rangle_0$, $a^\dagger_\alpha a^\dagger_\beta|g\rangle_0$, and $a^\dagger_\alpha a^\dagger_\beta a^\dagger_\gamma|g\rangle_0$ stand for the ground, single, double, and triple excited states of the uncoupled system, respectively. An alternative perturbative corrections to the LR-DFT excitation energies were proposed recently by Ziegler *et al.* [76,77].

Double excited states do not appear when TDA is invoked, and exchange-correlation coupling terms $\boldsymbol{V_{\alpha\beta\text{-}\gamma}}$ vanish. As a result, state-to-state transition dipoles coincide with the ones obtained in the CIS method, defined by the first term of eq. (10). Recently we suggested [100] to apply Tamm-Dancoff approximation and annihilate $\boldsymbol{Y}$ component of transition density *a posteriori*, after LR equation had been solved. Thus, excitation energies and ground to excited transition dipoles remain unaffected, while CIS formulas are applied to calculate

state-to-state transition dipoles and differences $\overline{\mu}$ between the permanent excited and ground state dipole moments:

$$\mu_{\alpha,\beta} = Tr(\mu(I-2\rho)\xi^*_\alpha\xi_\beta)\,;\ \overline{\mu}_\alpha = Tr(\mu(I-2\rho)\xi^*_\alpha\xi_\alpha)\,;\ \xi = \begin{bmatrix} X \\ 0 \end{bmatrix} \quad (14)$$

In addition, the double excited states $|\alpha\beta\rangle$ are introduced with the following excitation energies and transition dipoles:

$$\Omega_{\alpha\beta} = \Omega_\alpha + \Omega_\beta\,;\ \mu_{0,\alpha\beta} = Tr(\mu(I-2\rho)\xi_\alpha\xi_\beta)\,;$$

$$\mu_{\alpha,\alpha\beta} = \mu_\beta\,;\ \mu_{\gamma,\alpha\beta} = 0 \quad (15)$$

We called this scheme *a posteriori* Tamm-Dancoff (ATDA) approximation [100]; it is intermediate between TDA and full second order TD-DFT. ATDA allows to calculate second order properties without solving equations of the full QR-DFT, using a simple modification to existing LR codes. Unlike QR-DFT, ATDA inherits double excited states from second order CEO formalism. In the Subsections 2.2-2.3 we demonstrate accuracy of ATDA in calculation of transition dipoles between excited states in trans-butadiene, as well as permanent dipole moments for the excited states in para-nitroaniline, and compare the numerical values with the ones obtained at higher theory levels. Comparison of the one-photon and two-photon absorption spectra for some chromophores with experimental data, made in the Subsection 2.4, illustrates the ability of the ATDA to reproduce optical properties with a good accuracy.

2.2. Benchmarking ATDA study of the transition dipole moments

Conjugated hydrocarbons (also known as polyenes) and their derivatives present an important class of compounds with rich photophysical and photochemical properties. These properties originate in a highly polarizable π-electron system and find a wide use in organic electronics [78] and photonics [79] applications. Another reason for interest in electronically excited states of polyenes is their role in biological processes of vision and photosynthesis. Theoretical description of electronic structure and electronic excited states in conjugated molecules plays a critical role in understanding the natural and engineered processes, and may assist in the rational design of the new materials with improved properties.

Polyenes often served as a testing ground for new theoretical methods, and comprehensive review of the published results seems to be impossible. Presently consensus is reached about ordering of the lowest excited states, with $2A_g$ one being above $1B_u$ (but close in energy) for trans butadiene and all-trans hexatriene, and below the $1B_u$ state for the higher hydrocarbons. Transition dipole moments between excited states of polyenes were much less studied, and double-excited nature of $2A_g$ states is still a matter of discussion [51]. At the same time, double-excited nature of selected excited states remains to be an important challenge of TD-DFT [47]. These aspects of electronic structure, as well as the ability of TD-DFT methods to describe them present one of the focuses of this review.

Accurate numerical values of transition dipoles between excited states of molecules are important for prediction of nonlinear photonic processes [80,81], such as excited state absorption and 2PA. States, involved in these processes, are often not observable in linear absorption spectra and some of them appear to possess strong double excited character [82-84]. The relation between two-photon absorption and other nonlinear optical properties of the ground sates is provided by the Sum over States (SOS) expression, derived within the perturbation theory approach [85]. Several authors [86-88] had noticed that first and second hyperpolarizability values, obtained for the linear polyenes at a semiempirical theory level within the SOS approach, are dominated by contributions from a few, so called "essential" states, so that all other states can be excluded from consideration. This approximation appeared attractive for structure-property relationship schemes [89,90], but later *ab initio* studies [66,91] reported it to be an oversimplification. In this Subsection we review the results of a more advanced correlation treatment [92], and identify approximations responsible for disagreements between different *ab initio* approaches.

In this Section we aim to focus on the valence ππ*-excited states, which are primarily responsible for the second and higher polarizabilities of conjugated hydrocarbons. Linear all-*trans* polyenes are planar molecules of C_{2h} symmetry, their π-orbitals belong to a_u and b_g irreducible representations. Configurations (Slater determinants) describing the electron transitions between the orbitals of the same symmetry contribute to A_g states, while transitions between the orbitals of different symmetry contribute to B_u states. Since the ground state is $1A_g$, one-photon transitions to B_u states are dipole-allowed and to A_g states are dipole-forbidden in the one-photon regime, while two-photon transitions are forbidden to B_u states and allowed to A_g states. Besides the spatial symmetry, π-states can be classified according to the so-called alternacy, or particle-hole symmetry [93]. It is exact only with some model Hamiltonians (Huckel or Parriser-Parr-Pople), and becomes approximate after σ-π and second-neighbor interactions are included. However, it is useful for interpretation of transition dipoles from *ab initio* calculations. Let us first introduce shorthand notations *1, 2, ..., m* for the occupied and *1', 2', ..., m'* for the vacant π-orbitals, with HOMO being *1*, and LUMO being *1'*. When model Hamiltonians are used, configurations *m→n'* and *n→m'* are degenerate and therefore contribute equally to the state wavefunction. Their in-phase and anti-phase linear combinations give rise to *plus* and *minus* states [94] The valence bond theory description of in-phase states [95] includes a substantial contribution from ionic resonance structures, while for the anti-phase states it does not. For this reason *plus* and *minus* states are often called *ionic* and *covalent* respectively [96]. The actual sign of the amplitude for every given configuration depends on the signs of singly occupied orbitals included in this configuration and is assigned arbitrary in most of software packages. Hence, we will use *ionic* and *covalent* notations, as *plus* and *minus* notations tend to be misleading. Similar to the spatial symmetry, the alternacy symmetry results in selection rules for one-photon transitions, as the dipole transition moment between any two *ionic* states or between any two *covalent* states is zero. The ground state $1A_g$ behaves like a *covalent* state. The excited configurations of the type of *m→m'* behave like *ionic* states for singlet-spin states and *covalent* states for triplet-spin states. The doubly excited configurations of *mm→n'n'* type behave like *covalent* states and mix with the singly excited *covalent* configurations. This results in multiconfigurational character of the *covalent* $2A_g$ state and explains why this state is strongly stabilized, sometimes below the *ionic* $1B_u$ state, of predominantly *1→1'* nature.

Ab-initio description of the molecular excited states typically starts with molecular orbitals, optimized in the self consistent field (SCF) procedure with a single Slater determinant wavefunction of the ground state, known as the restricted HF method. Excited states can in principle be described by single determinants (or a couple of determinants, for open shell singlets), which are constrained to be orthogonal to Slater determinants of the lower-lying states. While this approach works reasonably well at the DFT level [26,97], the HF description of excited states is generally inaccurate. Instead, configuration interaction (CI) methods are used, where one or more orbitals in the HF determinant are substituted with unoccupied orbitals to form excited configurations. The

wavefunction of the system is expressed as a linear combination of these configurations and electronic states are found by diagonalization of the Hamiltonian. All possible substitutions in the HF determinant yield the Full Configuration Interactions method (FCI). It gives an exact solution to the Schrödinger equation for a given atomic basis [98]. The exponential growth of the computational effort with the size of the system makes FCI attainable only for very small molecular systems, and for practical reasons various truncation schemes are introduced. The simplest scheme restricts the expansion of the wavefunction to single substitutions (CI Singles, or CIS), another one limits the substitutions to singles and doubles (CISD). To reduce the computational effort, amplitudes for double substitutions can be evaluated perturbatively (instead of the variational approach), resulting in the CIS(D) method [99]. When applied to the ground state, the method is known as MP2 (Moeller-Plesset second order perturbation theory). Second-order Algebraic Diagrammatic Construction presents yet another perturbation correction method, where the correction is applied to the matrix elements before solving CIS equations [100]. Variational CISD description for the ground state is known not to be size-consistent, which decreases its accuracy for the larger molecules. In order to maintain size-consistency, selected triple and quadruple excitations are added to the wavefunction in the form of products of single and double excited configurations. Their amplitudes are also taken as products rather than evaluated independently. This approach results in coupled cluster expansions (CCSD, CC2, etc.) [101]. At the moment couple cluster methodology provides arguably the best accuracy/cost ratio among wavefunction based methods. The CI method, based on the CC reference (SAC-CI) [102,103] extends this treatment to the excited states. Both single and double (SD-R) [104] and up to sixth-order (General-R) [103] excitation truncation schemes were developed. Both SD-R and General-R were shown to yield similar results for the $2A_g$ state of trans-butadiene.

The results for the singlet ππ*-states of butadiene are presented in Table 1. The reader can find these and other results on hexatriene and octatetraene in Ref. [92]. The chemical structure of trans butadiene is shown in Scheme 2.

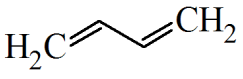

Scheme 2. Trans-butadiene.

A close examination of the major configurations in the SAC-CI wavefunction reveals that the alternacy symmetry classification into *ionic* and *covalent* states approximately holds. Out of two linear combinations of (*i*-*j*') and (*j*-*i*') determinants, the *covalent* combination is lower in energy and contains a larger contribution from the double excitations. The actual signs of the amplitudes depend on the phase of molecular orbitals, and are therefore arbitrary. For *covalent* A_g states, one can observe a large transition dipole from the *ionic* $1B_u$ state. For *covalent* B_u states, transition dipoles from the *covalent* ground state are much lower, than for *ionic* B_u states, according to alternacy selection rules. As one can see from SAC-CI wavefunction analysis, this stabilization of the *covalent vs. ionic* state corresponds to 7-14% contribution from the leading double excited configuration, which is found insignificant in *ionic* states. The same stabilization is paralleled by both CIS(D) and TD-DFT excitation energies. For instance, in hexatriene the CIS *covalent* $2B_u$ state is 0.5eV above the *ionic* $3B_u$ state, the CIS(D) *covalent* $2B_u$ state is 1.5 eV below the *ionic* $3B_u$ state. Similarly, the ATDA *covalent* $2B_u$ state is 1 eV lower than the *ionic* $3B_u$ state. While this stabilization is achieved through the perturbative correction for double excitations in case of CIS(D), it is afforded by means of the exchange-correlation potential in the case of TD-DFT. Comparison SAC-CI with CIS results, where *covalent* states are systematically destabilized with respect to *ionic* states, is especially instructive.

Thus, analysis of SAC-CI wavefunction, which includes both static and dynamic electron correlations shows that double-excited character of $2A_g$ and other lower-lying *covalent* states in the linear polyenes is relatively weak (less than 20%) and these states can be therefore classified as predominantly single excitations. This is in contrast with *ionic* states that have purely single excited character. Some of the higher-lying states however have considerably higher contributions of the doubly excited configurations (40-80%). Excitation energies of these states are close to the sum of the excitation energies of the respective predominantly single excited states. Even though doubly excited configurations appear to contribute much less than 100% to the wavefunction, this contribution is more than twice greater than the one observed in predominantly single excited states. Thus, these states can be interpreted as predominantly doubly excited. This interpretation is confirmed by the trends in excitation energy and transition dipoles, as described below. Thus, single and double excitations in linear polyenes at the equilibrium geometry are separated by a gap in double excited character (below 20% and above 40%). It is conceivable that far from equilibrium this observation may not hold.

Let us consider the $4A_g$ state of butadiene as an example. According to Table 1, $4A_g$ has excitation energy of 12.6 eV, close to the double excitation energy for the $1B_u$ state (6.8 eV). Meanwhile, its leading configuration (11-1'1') corresponds to the double HOMO-LUMO excitation (1-1'), which is the leading configuration in the $1B_u$ state. Similarly, the $3B_u$ state of butadiene with the leading configurations of (11-1'2')-(12-1'1') originates from the product of singly excited $1B_u$ (1-1') and $3A_g$ (1-2')-(2-1') states. Its excitation energy of 15.3 eV is nearly equal to the sum of the respective excitation energies of 6.8 and 9.4 eV.

The relationships observed in SAC-CI results are closely resembled by the ATDA-B3LYP level of theory. The $2A_g$ and other states, appeared to be predominantly single excitations with SAC-CI, were found to have the excitation energies closer to benchmark values than uncorrected SAC-CI/DZp values. Unlike CIS(D) and SAC-CI results, *covalent* states are stabilized relative to the corresponding *ionic* states without explicitly including double excited configurations into the description. This confirms that the same electron correlation effects, which are described by double excited configurations in the wavefunction, are accounted for by the approximate exchange-correlation functional B3LYP. On the other hand the states, interpreted as predominantly doubly excited, are well reproduced by the second order CEO extension to TD-DFT, after eqs. (6–10) are simplified with ATDA. These states are completely absent in the list of CIS and CIS(D) states. It is necessary to stress, that double excited states are not present in the output of standard computer codes, implementing TD-DFT in either linear or quadratic response.

Transition dipole moments calculated with ATDA-DFT are in better agreement with SAC-CI values than CIS ones. They also compare favorably with QR-DFT results. While ground to B_u transition dipole moments are the same at ATDA and QR-DFT methods (being LR values), $1B_u$ to nA_g transition dipoles are different. Figure 2 illustrates the comparison of $1B_u$ to nA_g transition dipoles in butadiene obtained in the ATDA, QR-DFT, and SAC-CI. Ionic states are almost equally dark with QR and ATDA. *Covalent* A_g states of mostly single excited character are bright in SAC-CI, darker with ATDA, and even darker with QR. Covalent states of mostly double excited character are completely absent in QR, but their transition dipoles are borrowed by other states close in energy. Even with this in mind, ATDA values are still closer to SAC-CI ones.

Table 1. Excitation energies ΔE (eV), major contributing configurations, and % contributions of the leading double excited configurations for the lowest π-states of trans butadiene. Transition dipoles μ (a.u.), from the ground state to nB_u states, and from $1B_u$ to nA_g states are also reported. All basis sets are DZp. The benchmark values of excitation energies obtained at CAS-PT2/ANO are taken from Ref. [105].

	State	$1B_u$	$2B_u$	$3B_u$	$2A_g$	$3A_g$	$4A_g$	$5A_g$
CIS	ΔE,eV	6.66	12.15	-	9.66	9.03	-	-
	Config.	(1-1')	(2-2')	-	(1-2')+(2-1')	(1-2')-(2-1')	-	-
	μ,a.u.	2.661	0.784	-	2.682	0.112	-	-
CIS(D)	ΔE,eV	6.77	11.33	-	7.95	9.28	-	-
SAC-CI (SD-R)	ΔE,eV	6.86	11.72	15.31	7.51	9.41	12.65	16.71
	Config.	(1-1')	(2-2')+(11-1'2')	(11-1'2')-(12-1'1')	(2-1')+(1-2')+(11-1'1')	(1-2')-(2-1')	(2-1')+(1-2')-(11-1'1')	(12-1'2')+(22-1'1')+(11-2'2')
	%D	0	2	78	13	0	53	83
	μ,a.u.	2.291	0.874	0.17	1.695	0.306	2.698	0.557
ATDA-B3LYP	ΔE,eV	5.94	10.33	14.52	7.11	8.57	11.89	16.28
	Config.	(1-1')	(2-2')	(1-1')((1-2')-(2-1'))	(2-1')+(1-2')	(1-2')-(2-1')	(1-1')(1-1')	(1-1')(2-2')
	μ,a.u.	2.131	0.706		1.485	0.086	2.131	0.706
QR-B3LYP	μ,a.u.				1.293	0.199	-	-
CAS-PT2/ /ANO	ΔE,eV	6.06	-	-	6.27	-	-	-

According to eq. (11–13), transition dipole moment between the single and the double excited state (including this singly excited state as its component) is equal to one from the ground to the second component of the double excited state. SAC-CI transition dipole values between respective states are close to this CEO relationship, which confirms our classification of covalent states into predominantly single and predominantly double excitations. The accuracy of ATDA in prediction of the permanent dipole moments is reviewed in the next Subsection.

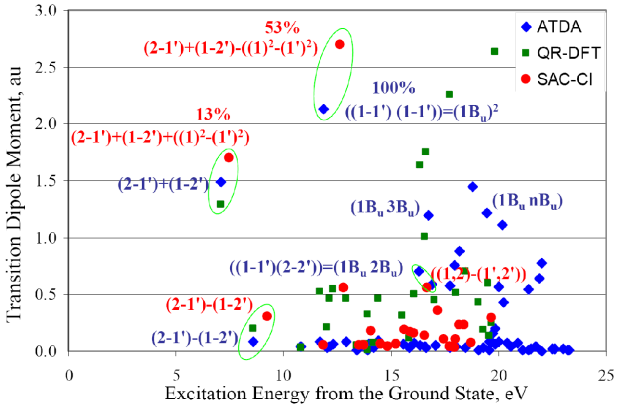

Figure 2. Calculated transition dipoles from $1B_u$ state to a manifold of nA_g states in trans-butadiene vs. excitation energy of nA_g states. With text labeled are configurations and percentage of double excitation. Color of the text correspond to the legend: red is for SAC-CI, and blue is for ATDA. Circled are the states of similar configuration in different methods. The first two A_g states below 10eV, obtained in the ATDA, are of single excited nature. All other ATDA states above 10eV with essentially non-zero dipoles correspond to double exited states constructed as ($1B_u$ nB_u).

2.3. Benchmarking ATDA study of the permanent excited state dipoles

In order to investigate the permanent dipole moments of the excited states in a prototypical donor/acceptor (D/A) substituted conjugated molecule, let us consider *para*-nitroaniline (PNA). Its structure is shown in Scheme 2.

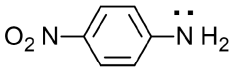

Scheme 2. Para-nitroaniline molecule.

PNA has a nonbonded electron pair localized on the amino group (which plays a role of donor) and a low-lying vacant antibonding orbital localized on the nitro group (electron acceptor). The π-conjugation through the six-membered phenyl ring allows for partial transfer of the electron density from the donor to the acceptor groups in both the ground and excited states. This electron mobility results in a number of properties important for organic electronics [78] and photonics [79] applications.

Photoinduced change in the permanent electric dipole moment reflects the degree of charge transfer resulting from electronic excitation [106], and is necessary for understanding of many practically important systems, from isolated molecules in the gas phase and in solution, to the band structures of organic semiconductors and crystalline materials, to complex biological systems [107]. Knowledge of the excited state dipole moments of PNA homologs is also important for wide variety of light induced charge transfer reactions [108].

Accurate numerical values of permanent dipole moments (as well as transition dipole moments) are also useful, along with transition dipole moments, for prediction of nonlinear optical properties with the SOS formalism [85]. The reliable estimation of nonlinear optical properties typically requires higher theory levels that include electron correlation. Prediction the dipole moments of the excited states was a challenge for TD-DFT [47]. However, in the previous Section, we have shown that ATDA to the second-order CEO formalism, applied to the TD-DFT can be used for an accurate, yet computationally inexpensive prediction of the transition dipoles. The focus of this Section is to analyze a performance of the ATDA method in prediction of permanent dipole moments of excited states based on comparison with the results obtained at a high-level wavefunction theory. As a test case, we analyze electronic structure of the five lowest excited states in each of four irreducible representation of the C_{2h} symmetry group of *para*-nitroaniline.

We optimized the geometry of *para*-nitroaniline in assumption of C_{2v} symmetry, at the CCSD/DZp level of theory. The B3LYP exchange-correlation functional was used in all DFT calculations. The basis set DZp, due to Nakayama *et al.* [109] was obtained by deleting *p*-functions on hydrogen from the correlation-consistent cc-pVDZ basis set [110] and used for all the calculations in this Section. The properties of the excited states in the EOM-CCSD method were obtained with the ACES2 program [111]. The permanent dipole moments at the QR-DFT level were obtained with the Dalton 2.0 [72]. The Gaussian 2003 suite of programs (revision E.1) [112] was used to perform TD-DFT calculations in two different ways. The numerical derivatives, according to Eq. (1) were calculated using the keyword 'Polar'. The calculations with the unrelaxed TD-DFT density were also carried out using the keyword 'Density=RhoCI'. A locally modified version of the Gaussian98 [113] was used for the calculations at the ATDA-DFT level of theory.

Properties of the five lowest singlet excited states for each irreducible representation within the C_{2v} symmetry are collected in Table 2. The properties include the excitation energies (ΔE), the projection of permanent dipole moments,

which coincides with the rotation axis in the C_{2v} point group, and leading electronic configurations of the excited states obtained at EOM-CCSD and TD-DFT theory levels. The EOM-CCSD excitations in each symmetry species are sorted by energies. For TD-DFT method the states are ordered by the close correspondence of their leading configurations to the leading configurations of the EOM-CCSD excited states. In order to describe configurations, we use the same shorthand notations for the occupied and vacant orbitals in each symmetry species as in the previous Section. The irreducible representations of the C_{2v} symmetry are assigned the following numbers: (1) a_1, (2) b_2, (3) b_1, (4) a_2. The number of irreducible representation is specified in brackets after the orbital. For instance, HOMO in the b_1 symmetry is labeled *1*(3), LUMO in the b_2 symmetry is labeled *1'*(2), and a configuration obtained from the HF determinant by excitation of an electron from one into the other is denoted (*1*(3)-*1*'(2)).

Close examination of the EOM excited states reveals that contribution of double-excited determinants to the lower-lying states of *para*-nitroaniline is relatively small (less than 4%). This is typical for the chromophores of the donor-acceptor type. All four methods of calculating the dipole moments within the TD-DFT formalism report different values for the same states. While Quadratic Response values are reasonably close to the numerical differentiation results, the permanent dipole moments for the TD-DFT obtained with the unrelaxed electronic density ('unrelaxed dipoles') are often overestimated. ATDA dipoles are in better agreement with the EOM results, especially for the lowest excitations in each irreducible representation.

The deviations of QR-DFT dipoles from the numerical derivatives for some states may be explained by a large discrepancy between QR-DFT and EOM-CCSD energies. The second order corrections for excitation energies are not calculated in the QR-DFT implemented in the Dalton 2.0. Permanent dipole moments are obtained in the QR formalism as a projection of the response function onto the energy spectrum calculated in the LR. For those states whose energies are not well-defined in the LR, i.e. their second order energy corrections are going to be large, the discrepancies in dipole moment values can be big. That deviation can be observed for near-degenerated levels, so that if energies of two states differ less that 0.1eV, they interfere in the QR formalism. Another possible explanation is switching the state ordering in the finite field used for numerical differentiation that can lead to incorrect calculation of the derivatives.

In order to quantify the differences between EOM-CCSD and TD-DFT excitation energies and permanent diploes, we calculated the standard deviations. They are reported in the last two rows of Table 2

One can see that numerical derivatives, QR-DFT and ATDA-DFT values are close to each other and to coupled cluster values, while unrelaxed dipole moments deviations are three times as large. We find ATDA-DFT, QR-DFT and numerical energy derivatives to be in good agreement with the results obtained with the EOM-CC approach. Unrelaxed density TD-DFT calculations, on the other hand, yield numerically inferior results. This validates the accuracy of ATDA for the description of permanent dipole moments of excited states in donor-acceptor molecules, exemplified by *para*-nitroaniline. We will review the applications of ATDA to prediction of the nonlinear optical properties in the next Subsection.

2.4. Application of ATDA to predict two photon absorption profiles for fluorene-based chromophores

2PA is an electronic excitation process involving simultaneous absorption of two photons. There are a wide range of 2PA applications, such as three dimensional data storage, photonic devices, lithographic micro-fabrication [114], quantum information technology [115], optical limiting, two-photon pumped lasing in organic chromophores and quantum dots [115,116], in-vivo bioimaging, and cell-selective photo-dynamic therapy [116]. Most applications require chromophores with large 2PA cross-sections to minimize laser intensity requirements and prevent overheating of targets [114]. To design more efficient 2PA chromophores, it is important to understand their structure/activity relationships (SARs). Computer modeling of 2PA spectra facilitates understanding of these relationships and is becoming an important part rational approach that may accelerate progress in the chromophore design [90]. Accurate predictions of 2PA spectral profiles would greatly assist in the design of more effective 2PA chromophores while eliminating poor candidates from the synthetic pipeline. The goal of this study is improvement in quantitative predictions of 2PA, as well as development of qualitative tool to assist in understanding the relations between the electronic structure of the chromophores and 2PA profiles in terms of the transition dipole moments and state energies.

In the past decades several research groups had made a strong effort aimed at the development of new compounds with large 2PA cross-sections. The main guiding principle used in those studies involved the electron transfer between electron-donor (D) and electron-acceptor (A) moieties attached symmetrically or asymmetrically to the π-conjugated bridge. The fluorene fragment in particular was found to be a good example of the π-conjugated bridge due to the highly delocalized π-system delocalized over the two benzene rings held together at a nearly coplanar orientation by the methylene bridge [117]. *D*-π-*A*, *D*-π-*D*, or *A*-π-*A* molecular structures have been proposed and studied both theoretically and experimentally. In studies by Belfield *et al.* fluorene derivatives have been extended to *D*-π-π-*A* and *A*-π-π-*A* types with the aim of increasing 2PA absorption cross-sections [118-123]. However, the choice of functional groups and linkages, the most appropriate for developing chromophores with large 2PA characteristics, is still under active investigation [124-135].

In order to accelerate experimental efforts based on the traditional trial and error approach, a quantitative understanding of the trends in dependence of the 2PA cross-section on a molecular structure would be clearly beneficial. Two major approaches have been used to accomplish that goal. The first one is based on essential state models (three-state, four-state, etc.). Parameters of these models (such as excitation energies and transition dipoles) are adjusted to fit experimental data. These parameters are then correlated with details of the molecular structure (π-conjugated chain lengths, donor/acceptor strengths, etc.). Another approach consists of quantitative prediction of 2PA cross-sections at a chosen level of theory, followed by analysis of the physical principles of the major contributions into this property. The levels of theory, used for 2PA predictions cover a wide range.

In recent quantum chemical calculations performed on conjugated chromophores have shown that a substantial symmetric charge redistribution that occurs upon excitation may account for a heightened sensitivity to 2PA events [118]. In their work Bredas *et al*. established good agreement between the peak values of 2PA cross-sections measured with femto-second pulses and those calculated with the semi-empirical intermediate neglect of differential overlap Hamiltonian with multi-reference double-configuration interaction (INDO-MRD-CI) scheme based methods. Aside from the donor-acceptor configuration of 2PA active chromophores, it was also established by Bredas *et al.* that increasing the length and charge transfer of the molecules results in an increase in 2PA cross-sections and may also result in a significant shift of 2PA to longer wavelengths [118]. In another

Table 2. Excitation energies ΔE (eV), permanent dipole moments, and leading electronic configurations for the lowest excited states of para-nitroaniline at the EOM-CCSD theory level and four formalisms at the TD-DFT level. The % of the double excited character is reported for EOM-CCSD states and the numbers of the excited state in each symmetry species are reported for TD-DFT calculations. The ground state dipole moment is calculated to be 2.66 and 2.86 a.u. at CCSD and DFT levels of theory, respectively.

Symmetry	EOM-CCSD			
	ΔE, eV	Configurations	%D	μ, a.u.
A_1 (1)	4.92	(1(3)-1'(3))+(2(4)2(4)-1'(3)1'(3))-(1(3)1(3)-1'(3)1'(3))-(1(3)1(4)-1'(4)1'(3))	0.9	5.65
	6.99	(1(3)-2'(3))+(1(4)-1'(4))-(1(3)1(3)-1'(3)1'(3))	0.3	4.64
	7.48	(1(4)-1'(4))-(1(3)1(3)-1'(4)1'(4))+(3(3)1(3)-1'(4)1'(4))	1.0	3.22
	8.08	(2(3)-1'(3))+(1(3)-2'(3))-(1(3)1(3)-1'(3)1'(3))	2.3	4.60
	8.42	(2(4)-1'(4))+(1(3)2(4)-1'(3)1'(4))	1.5	-1.59
B_2 (2)	4.74	(1(3)-1'(4))+(1(4)-1'(3))-(1(3)1(3)-3'(3)1'(4))	0.3	3.25
	6.31	(1(4)-1'(3))-(2(4)-1'(3))-(1(3)-1'(4))+(1(3)2(4)-1'(3)1'(3))	0.3	4.03
	6.81	(2(4)-1'(3))+(1(4)-1'(3))-(1(3)2(4)-1'(3)1'(3))	1.6	2.49
	8.33	(2(3)-1'(4))+(1(4)-2'(3))-(1(3)1(4)-1'(4)1'(4))	0.3	5.04
	8.83	(1(4)-2'(3))-(2(3)-1'(4))+(1(3)1(4)-1'(4)1'(4))	1.4	2.88
B_1 (3)	4.76	(1(1)-1'(3))+(1(1)-2'(3))-(1(2)2(4)-1'(3)1'(3))+(1(2)2(4)-1'(3)2'(3))	0.9	2.03
	6.58	(1(3)-1'(1))+(2(3)-1'(1))	0.0	-0.16
	7.69	(1(3)-2'(1))	0.0	3.02
	8.04	(1(2)-1'(4))+(1(2)1(3)-1'(4)1'(3))	1.6	-1.54
	8.56	(2(2)-1'(4))	0.0	2.86
A_2 (4)	4.26	(1(2)-1'(3))+(1(2)-2'(3))-(1(1)2(4)-1'(3)1'(3))	0.5	1.92
	7.61	(1(3)-1'(2))	0.0	0.63
	8.18	(1(1)-1'(4))+(1(1)1(3)-1'(4)1'(3))	0.6	-0.75
	8.33	(2(2)-1'(3))	0.0	3.52
	8.64	(1(4)-2'(1))	0.0	1.19

Symmetry	TD-DFT						
	Root	ΔE, eV	Configurations	μ, a.u.			
				Numeric	Unre-laxed	ATDA	QR-DFT
A_1 (1)	1	4.09	(1(3)-1'(3))	4.93	7.61	5.56	4.93
	2	6.21	(1(3)-2'(3))-(1(4)-1'(4))	3.59	4.42	3.66	3.60
	5	6.98	(1(4)-1'(4))+(1(3)-2'(3))+(2(4)-1'(4))+(2(3)-1'(3))	3.05	3.60	3.33	3.05
	4	6.62	(2(3)-1'(3))	5.06	5.96	4.34	4.61
	3	6.52	(2(4)-1'(4))	-0.30	-2.42	0.24	0.14
B_2 (2)	1	4.59	(1(3)-1'(4))+(1(4)-1'(3))	3.72	4.68	3.82	3.72
	2	5.12	(1(4)-1'(3))-(1(3)-1'(4))	4.74	6.41	4.69	4.74
	3	6.27	(2(4)-1'(3))+(2(4)-2'(3))	1.03	0.97	0.79	1.03
	4	7.23	(1(4)-2'(3))-(2(3)-1'(4))	3.69	4.58	3.74	3.69
	6	8.00	(2(3)-1'(4))+(2(4)-2'(3))+(1(4)-2'(3))	2.12	1.68	2.18	2.39
B_1 (3)	1	4.44	(1(1)-1'(3))	2.11	1.50	2.16	2.11
	2	5.96	(1(3)-1'(1))	-0.40	-1.15	0.83	-0.40
	4	6.92	(1(3)-2'(1))	2.77	3.26	3.06	2.77
	3	5.99	(1(2)-1'(4))	-0.15	-3.27	-0.21	-0.15
	6	7.91	(2(2)-1'(4))	2.83	2.86	2.86	2.83
A_2 (4)	1	3.96	(1(2)-1'(3))	1.99	1.27	2.04	1.99
	3	6.89	(1(3)-1'(2))	0.55	0.19	1.52	0.53
	2	6.35	(1(1)-1'(4))	-0.01	-2.91	-0.02	-0.01
	5	7.03	(2(2)-1'(3))	4.43	5.83	4.35	4.45
	7	8.09	(1(4)-2'(1))	1.87	1.61	-0.63	1.88
rmsd		from	QR-DFT	0.60	2.08	0.70	-
		from	EOM-CCSD	0.98	1.58	0.96	0.90

study by Agren *et al*. [117] four lowest excited states of π conjugated systems were theoretically investigated using using the *ab initio* response theory. The materials were synthesized and characterized by Kim *et al.* [123] and Ventelon *et al.* [122] Agren *et al*. showed that their theoretical findings were consistent with the correlation between large 2PA cross-sections and a π center. Although 1PA spectra were strongly correlated to the molecular length, this was not always the case for 2PA in the visible domain [117]. Yet another study by Fabian *et al.* established that spectral absorption features are reasonably well reproduced by the approximate semi-empirical MO-CI methods based on the NDO (ZINDO/S), however the TD-DFT response theory proved to be superior over semi-empirical methods [136]. Since then Hales *et al.* showed that 2PA spectra for symmetric and asymmetric fluorene derivative compounds exhibit an intermediate resonant enhancement of nonlinearities, with an order of magnitude enhancement for asymmetric cases, when compared to degenerate 2PA. Semi-empirical methods that we based on on INDO-MRD-CI theory level and implemented a simplified three level model, were also shown to provide additional insight into the mechanisms governing 2PA events [137]. Several groups published works investigating the structure-activity relationships (SARs) responsible for these 2PA characteristics.

In this Subsection we review the recent prediction of 2PA cross-sections published recently [138]. The conjugated chromophores selected in that study to illustrate the accuracy of ATDA method, are presented in Scheme 3. Theoretical models of these were derived by truncation of the aliphatic chains and replacing them with to methyl groups in the original experimental structures. The abbreviations of the model molecules and the systematic names of the corresponding experimentally studied ones are: **1a**: 2,7-Bisbenzothiazolyl-9,9-didecylfluorene; **1b**: 2,7-Bis[4-(9,9-didecylfluoren-2-yl)vinyl]-phenylbenzothiazole; **1c**: 9,9-didecyl-2,7-bis(N,N-phenyl amino)-fluorene; **1d**: (7-benzothiazol-2-yl-9,9-didecylfluoren-2-yl)diphenylamine**;** **1e**: (7-[2-(4-Benzothiazol-2ylphenyl) vinyl]-9,9 didecylfluorene-2yl)diphenylamine. These compounds were experimentally synthesized and characterized by Belfield *et al.* as a model compounds for possible applications in two photon microfabrication, two photon photochemical transformations, non-destructive 3-D multiphoton fluorescence imaging, and photodynamic therapy [119,137,139]. These compounds exhibit large (600GM) cross-sections for **1a** while studying the design of rigid-rod polymers while 2PA cross-

sections of the polymers were reduced by aggregation [140]. Compound **1a** additionally exhibited a large fluorescence quantum yield. The good chemical, thermal, and photochemical stability, combined with desirable one- and two-photon absorption and luminescence properties, stand out as characteristics of this chromophore as a promising material for two-photon based technologies [141]. Compound **1d** has been previously implemented for in vivo 2PA biomedical imaging applications, as a fluorophore dye used for staining rat cardiomyoblast cells (H9c2), due to its high photostability, fluorescence quantum yield, and two-photon absorption cross-section over the tunable range of commercially available Ti:sapphire lasers [142]. Additionally, **1d** has been investigated as a potential 2PA free-radical photo-initiator for three-dimensionally resolved polymerization, resulting in intricate micro-fabrication and imaging [143].

Of the compounds in Scheme **3**, **1c** and **1d** have been previously studied theoretically by Hales *et al* using INDO-MRD-CI with geometries optimized with the AM1 semi-empirical Hamiltonian. All their calculations were carried out on isolated molecules and showed strong qualitative and quantitative agreement with experimentally generated spectra [137]. The three-level model developed in their study provided further insight into the mechanisms governing the nonlinear activity of 2PA active chromophores in relation to the description of the molecular states. A second study carried out by Day *et al.* implemented linear and quadratic response density functional theories to calculate the photo-physical properties of D-π-A molecules including **1d**. Their comparison of the two-state approximation and with calculation of 2PA via the SOS method including higher energy states drew a conclusion that the inclusion of higher energy states was necessary in description of 2PA [144,145].

In this Subsection we also use SOS approach, calculate state-to-state transition dipole moments μ_{nm}^{i} using ATDA as detailed in Subsection 2.1 and employ them to identify the essential states governing the 2PA process. Our aim is to validate ATDA by using these approximate μ_{nm}^{i} to predict the resonant 2PA cross-sections with SOS models and compare them to CEO results as well as experimental values.

Linear response TD-DFT allows one to obtain transition dipole moments and transition energies from the ground state to a manifold of excited states. These values are sufficient to calculate a 1PA spectrum. Predictions of 2PA are more involved. For a single linear polarized laser beam, the 2PA cross-section, averaged over isotropic molecular orientation can be expressed in cgs units as follows [146]:

$$\sigma_{2PA} = \frac{8\pi^3\omega^2}{15c^2} g(2\omega) \sum_{a,b}^{3} \left(M_{aa} M_{bb}^{*} + 2M_{ab} M_{ab}^{*} \right) \qquad (16)$$

Here *a,b* = *x,y,z*, and *M* is so-called 2PA transition moment, expressed as the SOS via transition dipoles between the excited states:

$$M_{ij} = \frac{1}{2\hbar} \sum_{k}^{N} \left(\frac{\mu_{fk}^{i} \mu_{kg}^{j} + \mu_{fk}^{j} \mu_{kg}^{i}}{\omega_{kg} - \omega - i\Gamma/\hbar} \right) \qquad (17)$$

Here g(2ω) is the Lorentzian lineshape. In this expression, the summation runs over all the excited states; and the transition dipole moments between the *f*-th and *k*-th excited states (permanent dipoles, when $f = k$) are

$$\langle f | \overline{\mu_\alpha} | k \rangle = \langle f | \mu_\alpha | k \rangle - \langle 0 | \mu_\alpha | 0 \rangle \delta_{fk} \qquad (18)$$

To predict a 2PA spectrum one needs transition dipole moments between excited states and permanent dipole moments for infinite number of excited states. These values can be obtained only if one retains the terms quadratic in external field while solving the time-dependent equations. This quadratic approximation uses the states obtained in the linear response approximation as the basis, and involves summation over infinite number of these states. This summation can also be replaced by linear equations, as it is done in QR-DFT. Alternatively, one can carry out explicit summation over a sufficient number of the lowest excited states. The state to state transition dipoles and permanent excited state dipoles can also be approximated using ATDA, and substituted in eq. (16) to predict 2PA. Transition energies and ground to excited transition dipoles remain in ATDA identical to the ones obtained in full linear response TD-DFT calculations. At the same time, ATDA allows calculations of the state to state transition dipoles without solving the equations of full QR-DFT. Thus, it can be used for a computationally inexpensive prediction of linear and nonlinear properties of organic molecules. This ATDA/SOS approach opens new venues for interpretation of 2PA properties in terms of molecular electronic structure and can be used for rational design of 2PA chromophores.

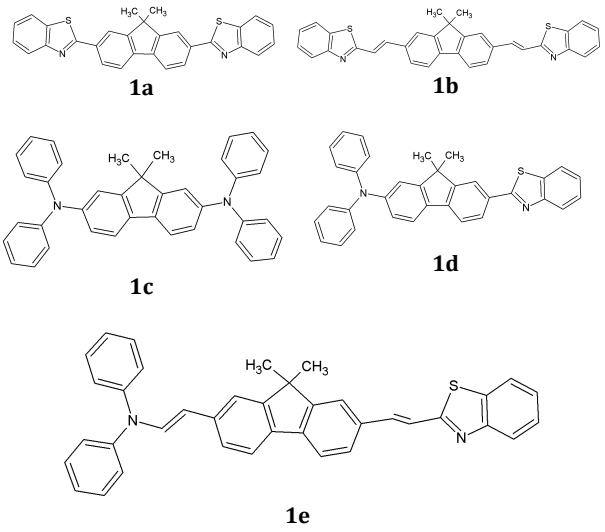

Scheme 3. Structural formulas of the molecules studied.

All molecular structures were optimized at the HF/STO-3G theory level, which favored planar geometry of conjugated molecules and was shown [147] to give the best agreement for the bond lengths as compared to the results of X-Ray diffraction experiments for stylbene and its three derivatives. The optimized geometries were confirmed by the absence of imaginary frequencies in the following normal mode calculations. The single point energy and transition dipole calculations were performed at the TD-B3LYP/MIDI! level.

Transition density matrices for the 24 lowest excited states, as well as Kohn-Sham operators on these transition densities were printed out. Contributions of the second and third derivatives of the exchange-correlation potentials into Kohn-Sham operators, and operators on the pair combinations of transition densities were neglected. The commercially available computational program Gaussian98 [113] was modified as described in previous studies [148] in order to enable this printout. The frequency-dependent orientationally averaged first- and third-order polarizability tensors were generated from the generated matrices using eq. (16), as implemented in CEO program [74]. Habitual empirical linewidth of 0.1 eV was

used for both 1PA and 2PA. To analyze the electronic structure of the excited states we used natural transition orbitals (NTO), which diagonalize the transition density matrix, and give the best representation of the electronic excitation in single-particle terms [149]. The graphical software XCrysDen [150] was used to plot NTOs.

We present 2PA resonant energies and cross-sections in Table 3 [138]. Figure 3 represents canonical orbitals, transition dipoles and excitation energies for compound 1a. For two of the molecules, the 1PA and 2PA profiles obtained with both SOS and CEO formalisms are presented in Figure 4, along with linear spectra, and the natural transition orbitals. SOS and CEO results (marked by solid lines on 2PA spectra in Figure 4) are in excellent quantitative agreement with each other, which provides a validation for the ATDA/SOS method. Predicted 2PA profiles also agree well with experimental ones. Experimental measurements of their spectral properties were reported in [140-142,151]. While for most molecules agreement between resonant maxima is better than 0.1 eV, in the case of **1e** theoretical bands are red-shifted relative to experimental ones by approximately 0.44 eV (55 nm). This can be explained by a greater conformational flexibility of the longer conjugated chain, and by a blue shift of the absorption spectra for non-planar conformations. Overall, agreement with experiment validates the use of TD-DFT as a part of rational design strategies directed toward new and improved two-photon absorbing materials.

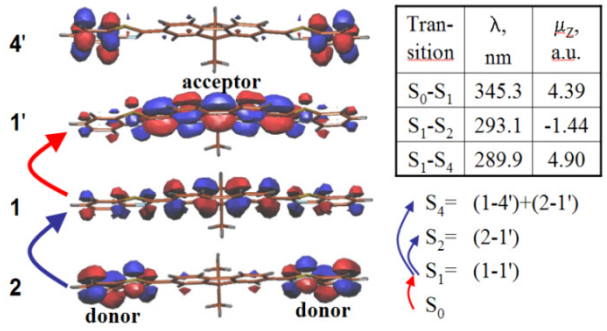

Figure 3. Canonical orbitals and orbital configurations of 2PA important excited states, their excitation wavelength (λ), and transition dipoles (μ).

We reviewed theoretical study [138] of five conjugated chromophores experimentally shown to have large two photon absorption cross-sections. The use of the third order response formalism within TD-DFT to calculate the frequency-dependent second order hyperpolarizability in both SOS and CEO methods to describe 2PA cross-sections resulted in very similar numerical values. The interpretive capabilities of these methods were different, however. While CEO expressions do not lend themselves easily to a quantitative analysis, SOS ones can be simplified to essential state models and employed to identify 2PA resonant states and interpret the relationships between the electronic structure and 2PA profiles. Natural Transition orbitals were also helpful to compare the electronic structure of the linear and two-photon absorbing states. State to state transition dipole moments, necessary for SOS expressions are calculated with ATDA and used to describe two-photon processes. Numerical values of the cross-sections obtained in SOS and CEO were found to be in good quantitative agreement with each other. Both SOS and CEO results are in good agreement with experiment. This validates the use of TD-DFT as a part of rational design strategies directed toward new and improved two-photon absorbing materials for bioimaging and optical data storage.

3. Density functional theory approach to photochemistry

3.1. Theory

In this Section we review DFT-based methods that can be used to simulate photochemical processes, such as light initiated bond breaking and formation. This task is far from trivial, as KS formalism of DFT was developed for non-degenerate cases; it breaks down for systems with strong diradical character and degeneracy of the electronic levels, such as CIX geometries. However, the static (also known as left-right) electron correlation can be taken into account by using different orbitals for different spin. This approach, known as unrestricted KS formalism is known to yield a qualitatively correct description of the bond breaking [153]. Alternatives to the broken spin-symmetry KS solution exist, including the multireference DFT [154], the local HF method [155], and the ensemble KS approach [156]. These new approaches, however, require development of new exchange-correlation functionals to obtain accurate numerical results.

Excited states, on the other hand, require the restricted formalism to avoid a heavy mixing of the higher spin states into description of the excited singlet. Although TD-DFT was suggested on the unrestricted KS reference [157], this is considered to be incorrect in a rigorous theory [158]. One possible approach to PES of the excited states can be formulated by adding the excitation energies obtained in the RTD-DFT formalism to the ground state energies calculated with the unrestricted KS method. Thereafter we will refer to this approach as to RTD-UDFT. Although for the photoswitching systems considered in this review the difference in the ground state energies obtained with restricted and unrestricted KS formalisms are close to within 20 kcal/mole or less, we will numerically show that this difference is sufficient to bring excited states PES to agreement with the results obtained at the higher theory level, when available.

At the first glance, the combination RTD-UDFT may appear contradictory. Let us remind the reader that the KS approximation to the DFT is semiempirical by virtue of the exchange-correlation potential used, including frequency (in) dependence of this functional to describe the excited states. The broken symmetry KS formalism compensates the deficiency of electron correlation description at the expense of spin contamination. The symmetry dilemma (broken symmetry or restricted) presents the choice of a lesser evil, and this choice need not be the same for the ground and excited states. While spin contamination is moderate and tolerable for the ground state, we found it to be prohibitive for the excited state perhaps due to the close proximity of the triplets and uncontrolled spin contamination.

Another theoretical development, necessary to describe the region of CIX is related to the double excited states, missing in the adiabatic linear response TD-DFT approximation [47]. Mixing of the double excited states to the linear response TD-DFT states through the so-called “dressed TD” was introduced recently by Burke, Maitra *et al.* [159] as a result of the particular frequency dependence for the exchange-correlation potential. However, a much more conceptually simple solution exists in the CEO formalism [73-75], where doubly excited states appear in the second order as simple products of the excitations obtained at the linear response level. This fact was used to propose ATDA, which we discussed in details in Section 2. State-to-state transition dipoles for butadiene and permanent dipoles for para-nitroaniline obtained in ATDA were compared with their values calculated with more sophisticated multireference methods. We also demonstrated good accuracy of the ATDA, comparing one- and two-photon absorption spectra for several chromophores with experimental data. Below we will review the studies [30] and

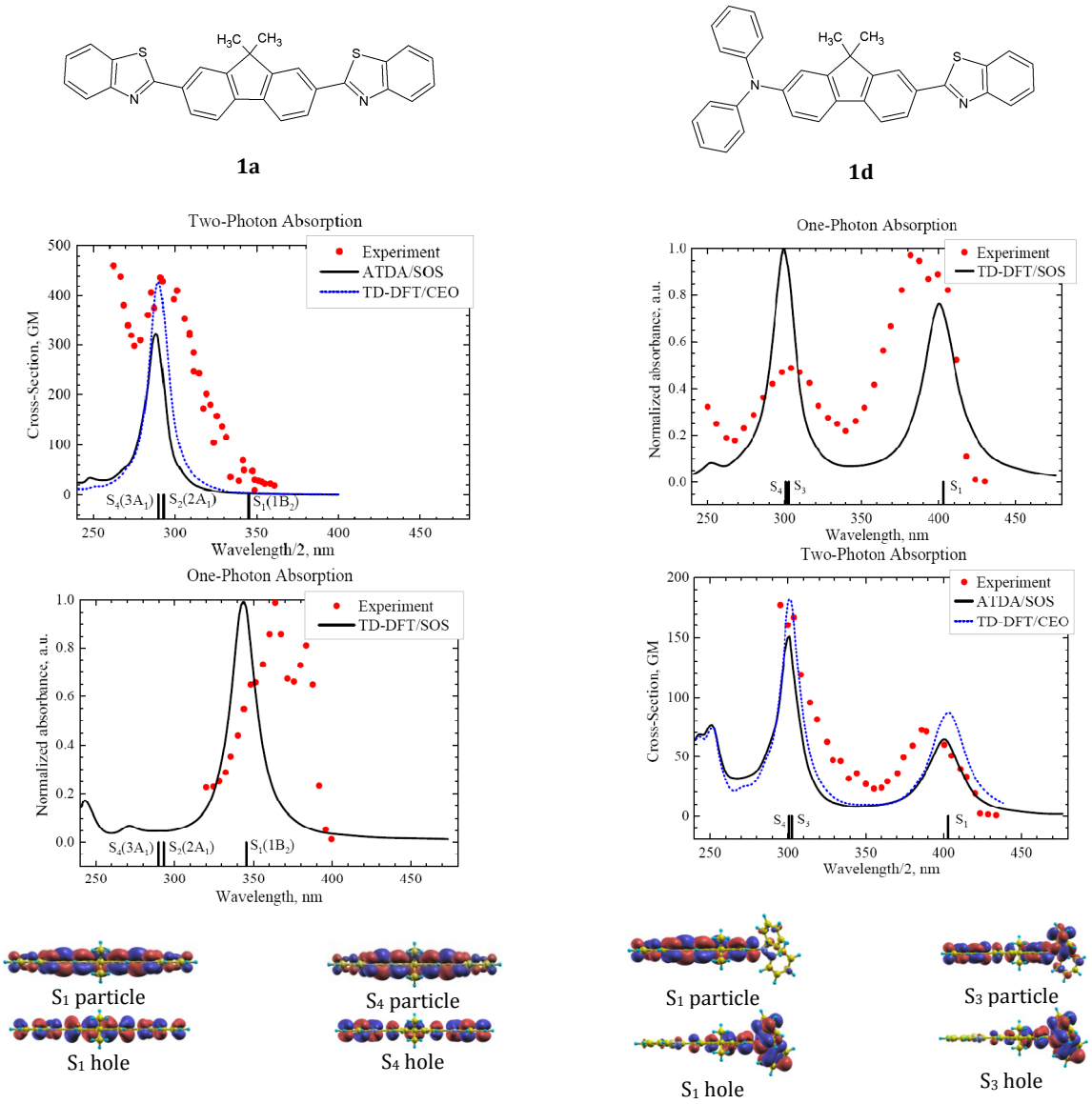

Figure 4. Structural formulas (top row), 1PA profiles (row 2), 2PA profiles (row 3), and isosurfaces for natural transition orbitals (bottom row) for studied conjugated chromophores. Diamonds mark the experimental profiles taken from [140] for **1a**, and from [137] for **1d**, solid lines correspond to theoretical predictions with SOS and CEO formalisms.

Table 3. Excitation energies (ΔE, eV), wavelength (λ, nm), and 2PA cross-sections (σ, GM) for the electronically excited states in the molecules studied. Experimental data are taken from (a) [140], (b) [137], (c) [152].

Compound	State	ΔE_{calc}	σ_{calc}	ΔE_{exp}	σ_{exp}	λ_{exp}
1a[a]	S_1	3.59	-	3.41	-	364
	$S_{2,4}$	4.28	324	4.27	437	290
1d[c]	S_1	3.08	65	3.21	73	387
	S_3	4.10	151	-	-	-
	S_4	4.12	151	-	-	-
1e[c]	S_1	2.83	154	3.24	162	383
	S_2	3.56	133	4.03	-	306
	$S_{6,7,8}$	4.25	445	-	-	-
1b[b]	S_1	3.06	-	3.08	-	403
	S_2	3.46	711	-	-	-
	S_4	3.99	-	4	-	310
	S_{11}	4.45	486	-	-	-
1c[b]	S_1	3.38	-	3.1	-	400
	S_3	3.88	126	4	89	310
	$S_{5,6}$	4.01	-	-	-	-
	S_{15}	4.6	162	-	-	-

[160], where ATDA-UDFT produced the accurate energies for the HOMO-LUMO double excited state in the entire range of the bond breaking reaction coordinate C1…C6 for some benchmark molecular photoswitches, provided that the molecular geometry corresponds to that state.

Since analytical gradients in the ATDA-UDFT approach are not yet implemented in the computer codes, the studies reviewd below use an approximation called Slater transition state (STS) method to optimize geometry of the excited states. In this method, half an electron is promoted from HOMO to LUMO and self-consistency is achieved with these fractional orbital occupations [161]. STS is known to be a good approximation to the corresponding ΔSCF excitation energy [162,163]. It can be further extended to the modified linear response DFT method [164], which yields a considerable improvement in description of the charge-transfer and Rydberg states, compared to the linear response TD-DFT approach. A practical advantage of STS is an easier SCF convergence, compared to the excited-state SCF convergence, which often presents a major problem [161] [23].

Studies [30] and [160] used the Gaussian 2003 Rev. E1 suite of programs [112], and hybrid meta-GGA exchange-correlation functional M05-2X from Truhlar's group [165]. This functional was designed for accurate description of both equilibrium geometries and transition states. Relaxed energy scans (RES) were built by means of the constrained optimization technique and used as approximations to the true minimum energy pathways [166]. The pericyclic C1…C6 bond (reaction coordinate) was fixed in the range from 1.4 to 3.6Å with 0.1Å step size. The ground singlet state 1A, was optimized at the UM05-2X/6-31G level of theory, while single 1B and double 2A excited singlet state geometries were optimized in the STS method. The STS method was implemented using equal fractional occupation numbers for HOMO and LUMO in the alpha-set only [to approximate geometry of the single excited state 1B, IOp(5/75=1, 76=2)], and both alpha and beta sets to approximate geometry of the double excited state 2A [IOp(5/75=1, 76=2, 77=1, 78=2)]. While the STS-UM05-2X/6-31G theory level gave reasonable estimates for molecular geometry, the SCF energies obtained at this level were found to have an insufficient accuracy. Instead, the excitation energies were taken from single-point calculations at the corresponding optimized geometry in ATDA for the lowest single excited state 1B and the lowest double excited state 2A. The excitation energies thus obtained at the ATDA-M05-2X/6-31G level, were added to the ground state energies obtained at UM05-2X/6-31G level of theory. Resulting ATDA-UM05-2X/6-31G//STS-UM05-2X/6-31G energies were plotted in Figure 6–Figure 10. The KS orbitals in Figure 11 were generated using VRML option in the Molden graphical visualization package [167].

3.2. Benchmark study of hexatriene

Cyclohexadiene/hexatriene conversion is the simplest example of an electrocyclic reaction. The dynamics of the cycloreversion in the CHD/HT system was repeatedly studied with the time-resolved ultrafast spectroscopy techniques [19,168]. The results are summarized in Ref. [17]. While a solvent may stabilize the ionic 1B state compared to the covalent 2A and 1A states, this does not have an appreciable effect on the CHD/HT conversion rate, while it slows down conformational isomerization of HT considerably [169]. To describe the detailed mechanism of this photoprocess, it is convenient to consider state correlation diagrams, briefly introduced below.

The CHD/HT system presents a textbook case of an electrocyclic reaction, considered in the very first publication of orbital symmetry conservation rules by Woodward and Hoffman [170]. Their pioneering work pointed out that in order for the HT→CHD transition to have a low activation barrier in the ground state (be thermally allowed), the HOMO should have bonding character with respect to the C1–C6 interaction, closing the ring. This condition is satisfied when HOMO lobes localized on C1 and C6 atoms overlap in phase during disrotatory motion of the terminal CH_2 groups. Thus, the HOMO symmetry controls stereochemistry of the thermal reaction product when substituents are present. Promotion of electron to LUMO in the photoactivated process inverses symmetry of the wave function. In this case conrotatory motion of HT (or CHD in cycloreversion reaction) is necessary for lobes on C1 and C6 atoms to overlap in-phase (Figure 5) and create no potential barrier along the reaction pathway, making the reaction photochemically allowed.

Longuet-Higgins and Abrahamson reformulated the rule in terms of state correlation diagrams [171] (Figure 5, center). These diagrams consider three electronic states of the HT/CHD system, classified as symmetric (1A, 2A) or antisymmetric (1B) with respect to the axis C_2, conserved along the conrotatory cyclization pathway. State 2A is the doubly excited state of the reactant (2 electrons on LUMO, 0 electrons on HOMO). It correlates with the ground state of the product, which has the same symmetry (1A), while the singly excited state of the reactant (1B) correlates with the singly excited state of the product (HOMO and LUMO occupied with 1 electron each). It is important to note that selection rules allow 1A→1B transitions in the 1PA regime, and the 1A→2A transition in the 2PA regime. Along the reaction pathway 1A raises, and 2A drops in energy. When approaching degeneracy, 1A and 2A mix to form an avoided crossing. This region forms a potential barrier on the ground state surface, and the so-called pericyclic minimum on the doubly excited state (2A) surface. Even though energy diagrams are drawn along the C_2-symmetric coordinate and clearly present an oversimplification, qualitative diagrams based on semiempirical Molecular Orbital calculations served as a useful guidance for the rational design of thermally irreversible photochromic molecules [5].

It is worth noting that σ and σ* orbitals of CHD, involved in the bond breaking process (Figure 5), are not frontier orbitals (HOMO and LUMO), unless the bond is elongated enough. As was stressed by Michl [172], the photochemical transformations are controlled by essential orbitals, which often do not coincide with frontier orbitals. This means that the photochemically excited state (usually the lowest singlet state of essentially HOMO→LUMO character) may increase in energy along the reaction pathway before it can proceed down to the pericyclic minimum. This may lead to an activation barrier which will slow down or prohibit the photochemical process. Thus, even simple orbital considerations can be used for semiquantitative prediction of the photochemical kinetics.

More accurate quantitative calculations, on the other hand, involve plotting realistic potential energy surfaces (PES), which until recently required the use of *ab initio* multireference-based quantum chemistry methods. Pioneering CAS study of HT/CHD system was published by Robb, Olivucci *et al*. [173-175]. They found that 2A and 1A surfaces touch at a molecular conformation of tetraradical character, located away from the C_2-symmetric coordinate, and including partial bonds C1…C6 and C2…C6. They also found that account for dynamic electron correlation is essential to correctly predict relative energies of 1B and 2A states.

Despite the fact that 2A/1A and 1B/2A conical intersections complicate the energy landscape by adding an extra dimension, qualitative interpretation given by the state correlation diagram along the symmetric coordinate still holds. It was further confirmed at the high level (CAS second order perturbation theory and multireference configuration interaction) by building *ab initio* PES and performing two-dimensional quantum dynamics [176,177] on this PES. A barrierless descent on the excited state PES was found to determine ultrafast photoconversion between CHD and HT, and

the quantum yield of this process was primarily determined by the location of 2A/1A CIX.

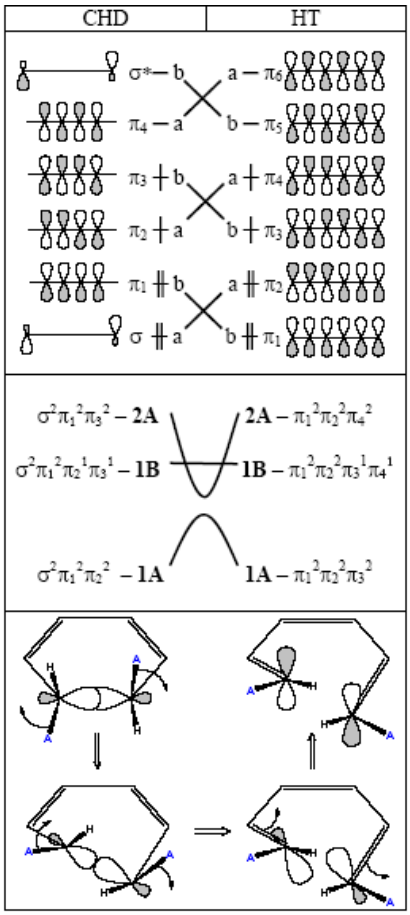

Figure 5. Orbital (top) and state (center) correlation diagrams for photointiated electrocyclic conversion of CHD to HT (bottom). Lines connect the orbitals as they continuously transform along the C_2-symmetric reaction path. Different orbital occupations give rise to different electronic states. The doubly excited state 2A of CHD correlates with the ground state of HT and vice versa; when their energies approach each pother, the states strongly mix and avoid crossing; a true CIX occurs away from symmetric coordinate.

Relaxed potential energy scans obtained in this study are plotted in Figure 6. They are in good agreement with high level *ab initio* results. As the C1…C6 reaction coordinate contracts from non-bonding distance to the normal covalent bond, the bright 1B state (characterized by a large transition dipole from the ground state), is being monotonically stabilized in energy, starting descent to the pericyclic minimum. At the same time the dark 2A state (with a negligibly small transition dipole from the ground state) is being stabilized even faster, crosses the 1B state surface, and forms the bottom of the pericyclic minimum.

It is worth noting that the geometry of the ground state does not approximate the excited state geometry accurately enough to produce a reasonable RES. The vertical excitation energy curve, plotted in Figure 6 and representing energy of the 1B excited state at the ground state geometry, displays a maximum instead of the pericyclic minimum, and contradicts both high level *ab initio* data, and the more accurate relaxed ATDA-UDFT data.

Qualitative comparison between our modified DFT results and a state-of-the-art wavefunction method, multi reference second order perturbation theory, calculations of the CHD/HT system is presented in Figure 7. Four important points were considered: equilibrium geometries for closed and open isomers (CHD and HT), corresponding to the Franck-Condon geometries of the ground states; and excited states 1B and 2A, optimized into the respective pericyclic minima. As one can see, ATDA-UDFT //STS-DFT at the M05-2X/6-31G theory level, adopted in this work, almost uniformly overstabilizes both excited states by 0.4–1.0 eV, but retains the correct order of the excited states, as compared to the multireference perturbation theory results. To the best of our knowledge, the correct state ordering in this system was not predicted by any other DFT-based approach.

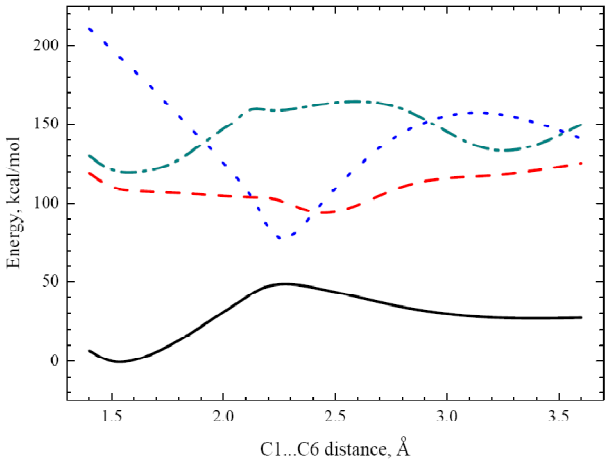

Figure 6. Relaxed potential energy scans for the ground (S_0, 1A – solid line), single excited (S_1, 1B – long dashes) and double excited states (S_2, 2A – short dashes) along the reaction pathway of the ring-closing C1…C6 bond in the CHD/HT system, predicted at the ATDA-UDFT/6-31G//STS-DFT/6-31G theory level, using the M05-2X exchange-correlation functional. The absence of an appreciable energy barrier on the pathway from the 1B state of CHD in the Franck-Condon geometry (left) to the minimum on the 2A surface is consistent with an ultrafast rate of the photoinitiated cycloreversion reaction CHD→HT. The upper dash-dotted line corresponds to the vertical single excitation at the optimized ground state geometry (S_1, 1A).

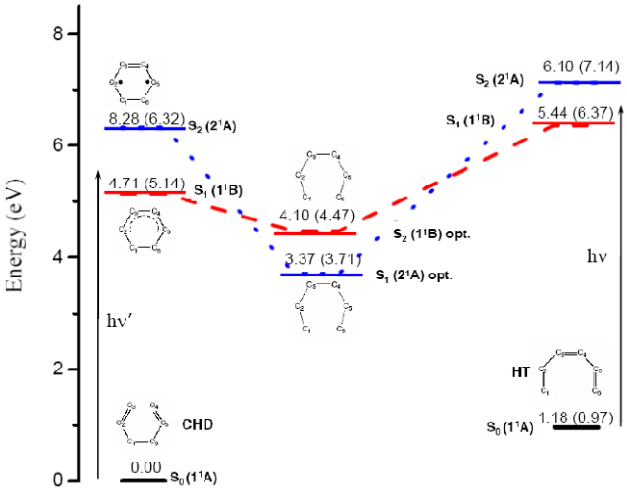

Figure 7. Relative state energies (in eV) for the ground and two lowest singlet excited states in the CHD/HT system, obtained at the ATDA-UDFT/6-31G//STS-DFT/6-31G theory level, using the M05-2X exchange-correlation functional. The results of high level ab initio calculations from Ref. [176] (multi-configurational quasi-degenerated perturbation theory) are shown for comparison in parentheses.

3.3 Benchmark study of dithienylethene

Dithienylethene (Scheme 1 with X=S) is the simplest homolog of diarilethens, an important class of compounds for photoswitching applications. In the closed conformation its thiophene rings are joined through the central bond to form a conjugated π-electron system. In the open form the π-conjugation between the rings is disrupted by the large

dihedral twists. The photochemistry of dithienylethene upon one-photon irradiation was studied in Ref. [9] using a molecular mechanics–valence bond computation. Dynamics was simulated on a hydrocarbon model system having the same potential energy surface topology as dithienylethene. The critical points were obtained at the CAS(10,10) theory level with basis sets 6-31G and 6-31G*. Dynamics was found to be essential to explain the observed photochemical behavior qualitatively. The authors claim, that the reaction path alone in insufficient for that purpose, as initial relaxation for this system was not directed toward CIX. However, the shape of the first excited state RES was found to be useful in interpretation of the ultrafast ring-closure and a relatively low quantum yield observed for the ring-opening reaction. Stepwise multiphoton processes in dithienylethene were studied in Ref. [178] The RES of several lowest singlet excited states were calculated at CAS(10,10)/6-31G and CAS(12,14)/6-31G theory levels. In all three of the excited states reported, the potential surfaces had a barrier to cycloreversion, located between the closed ring conformation and the pericyclic minimum. Although the crossover between excited states was not found in that study (presumably, due to neglect of dynamic electron correlation), the height of the barrier was found to be much lower in higher lying states. This fact was used to explain the experimentally observed sequential two-photon photoinitiation (via excited state absorption) in this system.

Our approximations of the minimum energy pathways for the ground and lowest single and double excited states are plotted in Figure 8. One can see that RES of the 1B state has a minimum in the closed form, and monotonically rises to the Franck-Condon region of the open form. The doubly excited 2A state, on the other hand, forms pericyclic minimum and crosses below the 1B state in the vicinity of CIX. Therefore, the excitation of the open form is followed by the ultrafast barrierless relaxation into the pericyclic minimum along 1B and then 2A RES, while the excitation of the closed form will populate the potential minimum on the excited state surface. The conversion of the excited closed form into the pericyclic minimum must first overcome a small (c.a. 5 kcal/mol) potential energy barrier, which leads to relatively slow cycloreversion. The excited state absorption will then bring the system from 1B to 2A state, followed by the barrierless relaxation toward the CIX. Thus, RES explain both slow cycloreversion and ultrafast photoswitching upon the sequential two-photon absorption.

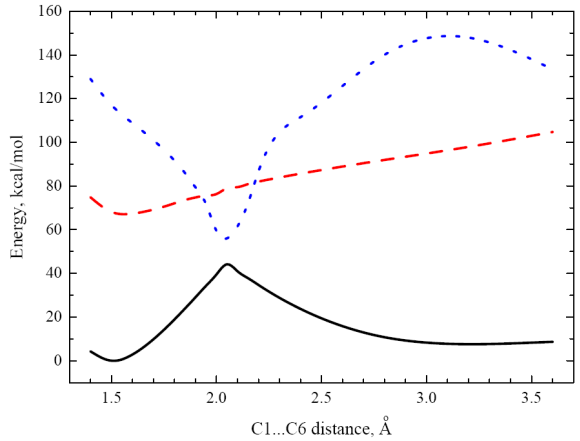

Figure 8. Relaxed energy scan for the ground (S_0, 1A), single excited (S_1, 1B) and double excited states (S_2, 2A) along the reaction pathway of the ring-closing C1...C6 bond in the dithioarylethene system, predicted at the ATDA-UDFT/6-31G//STS-DFT/6-31G theory level, using the M05-2X exchange-correlation functional. The legend is the same as in Figure 6.

3.4. Application to the prototype photoswitching molecule

Compound **2b** (Scheme 4) was recently synthesized by Belfield *et al.* [152]. They covalently attached the diphenylaminofluorene moiety to the compound **2a**. RESs for **2a** are plotted in Figure 9, and indicate that the excited state of the open form relaxes barrierlessly to the pericyclic minimum, while the closed form in its lowest excited state is separated from the pericyclic minimum by a sizable potential energy barrier. Therefore, ATDA-UDFT//STS-DFT method predicts **2a** to undergo ultrafast photochemical cyclization, while the cycloreversion is expected to be slow, in agreement with experimental data [179]. In the experiment, compound **2a** was doped into the polymer matrices (polyvinylcarbazol and polymethylmethacrylate). In either case the rate constant of the coloring process (cyclization) was found more than twice higher than the rate of the bleaching process (cycloreversion). The absorption spectrum of diarylethene 2a in the closed form has two bands (at 470–550 nm and 360–390 nm). TD-DFT calculations for gas phase yield the absorption maximum with a considerable blue shift, when compared to the experiment (the lowest vertical singlet excitations are at 423 and 324 nm for the closed ring geometry). Upon irradiation with visible light in the experiment, the first band disappears and the second one is considerably reduced in intensity. This is reproduced by TD-DFT calculations. The first singlet excited state for the open form 2a is at 386 nm, but the first excitation with sufficient oscillator strength is at 216 nm.

The diphenylaminofluorene substituent was designed similar to other fluorene-based donor-fluorene-donor and donor-fluorene-acceptor chromophores, previously shown to have a large 2PA cross-section [180,181]. Its attachment to the photoswitching core **2a** (Scheme 4) was expected to produce an enhanced photochromic compound designed to work as Write Once, Read Many (WORM) photoswitch in the two-photon absorbing regime.

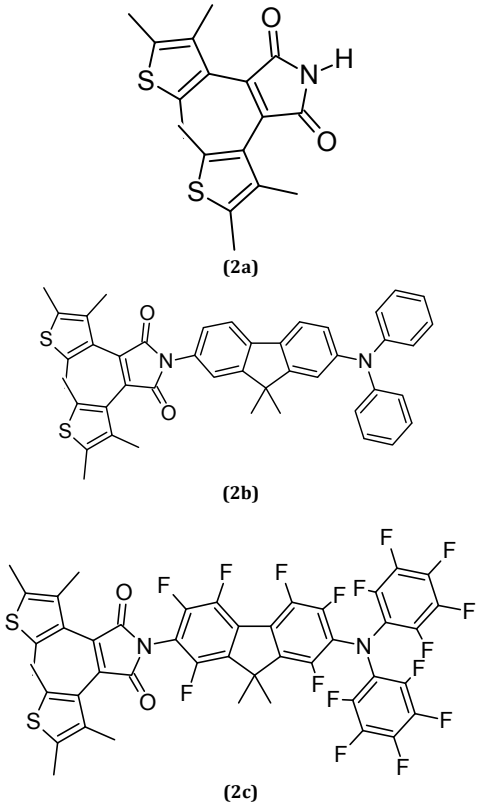

Scheme 4. Open forms of considered compounds.

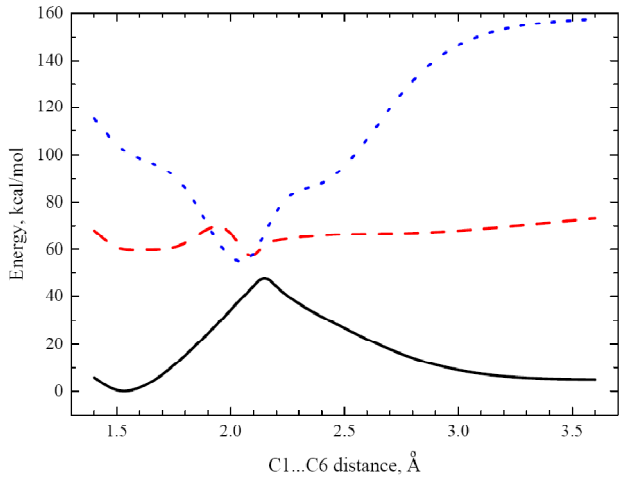

Figure 9. Relaxed energy scan for the ground state and the lowest single and double excited states in compound 2a (Scheme 4). The legend is the same as in Figure 6. There is no barrier along the single excited state from the open-ring Franck-Condon region toward the pericyclic minimum. Experimentally, this compound is photoreactive in the both closed and open forms, though the rate of the coloring process (cyclization) is higher than the rate of bleaching (cycloreversion).

While the compound **2a** was experimentally found to be photoreactive, the molecule **2b** did not display photochromic properties. ATDA-UDFT//STS-DFT approach, verified in the Subsections 3.2 and 3.3, was applied to the molecule **2b** in order to predict the RESs. The resulting curves are reported in Figure 10b. As one can see, RES of the lowest excited state forms minima for the both open and closed forms, separated from the pericyclic minimum by potential energy barriers of 4.7 and 8.0 kcal/mole respectively. As it was shown in the previous Subsections, the barrier for the closed form is typical for the other diarylethene derivatives. However, the barrier for the open form is unexpected and is responsible for the loss of photoswitching properties.

In order to determine the nature of this barrier, KS orbitals in these molecules were analyzed. This analysis found that while the essential orbitals (antibonding and bonding with respect to forming the new C–C bond) are respectively HOMO and LUMO in molecule **2a**, they are HOMO–1 and LUMO for molecule **2b**. At the same time HOMO in molecule **2b** is primarily the lone pair of the nitrogen atom and is localized on the diphenylaminofluorene pendant group (Figure 11), designed to increase the 2PA cross-section. In molecule **2a** the HOMO to LUMO excitation reduces the anti-bonding effect and creates a bonding one. This increases the bond order between carbon atoms closing the ring from –1 to 0 and allows the descent toward the pericyclic minimum on the excited state PES. On the other hand, in molecule **2b** the change in HOMO occupation has no pronounced effect on the ring closure. The antibonding electrons are kept on HOMO–1 upon the excitation. The placement of an electron into bonding LUMO increases the bond order from –1 to –1/2 with net antibonding effect remaining, which is apparently insufficient for initiation of the ring closure reaction. Therefore, the lowest excited state is no longer photoreactive. Not surprisingly, its energy raises along the reaction coordinate connecting the Franck-Condon region and the pericyclic minimum. This is exactly what was observed on RES plotted in Figure 10b.

Apparently, in order to restore the photoreactivity in the prototype molecule one needs to stabilize the lone pair of the donor substituent. This can be accomplished by chemical modifications of the pendant group with an electronegative substituent. If this stabilization is sufficient, the donor orbital will have the lower energy than both of the essential orbitals, and they become the HOMO-LUMO pair once again. The perfluorination of the pendant group should stabilize all the orbitals, localized on this molecular fragment. Indeed, it was shown to result in greated stabilization of the donor substituent lone pair, relative to the pair of essential orbitals. The modified prototype (molecule **2c**) is shown on Scheme 4. Comparison of the energy levels in the molecules **2b** and **2c** is presented in Figure 11. While perfluorination of the pendant group lowers energy for all the orbitals considered, the stabilization is the greatest for the lone pair orbital, localized primarily on this fragment.

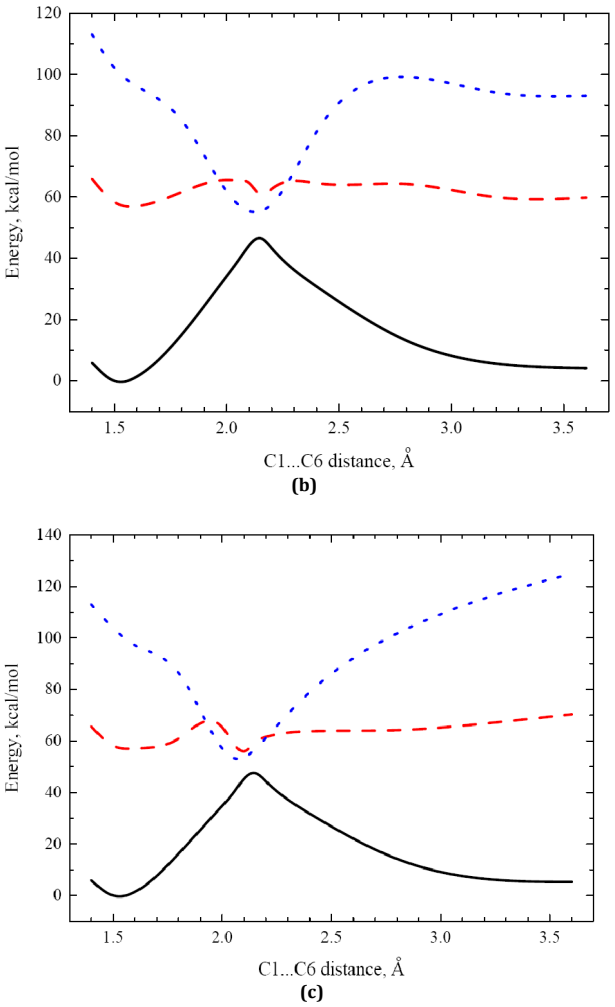

Figure 10. Relaxed energy scan for photocyclization in molecules **2b** (b, top) and **2c** (c, bottom), according to our results at the ATDA-UDFT//STS-DFT, M05-2X/6-31G level of theory. The legend is the same as in Figure 6. While for **2b** the both excited states exhibit potential energy barriers from the open isomer to the pericyclic minimum (b, top), there is no such a barrier in case of **2c** (c, bottom). This indicates that an ultrafast photoconversion is expected for **2c**.

The plot of RESs for the excited states in molecule **2c** (Figure 10c) confirms the essential orbital analysis. The energy of the lowest excited state is monotonically decreasing from the Franck-Condon region of the open form to the pericyclic minimum with no barrier. Thus, the electronic structure of the reactant can be used to predict the nature of the lowest excited state of the molecule, potential energy surface for this excited state, and the photochemical kinetics of electrocyclization. Based on the electronic structure of the systems considered in this Subsection, a general design principle for the photochromic molecules was formulated [30]: substituents should not introduce any electron energy levels within the HOMO-LUMO gap between the essential orbitals.

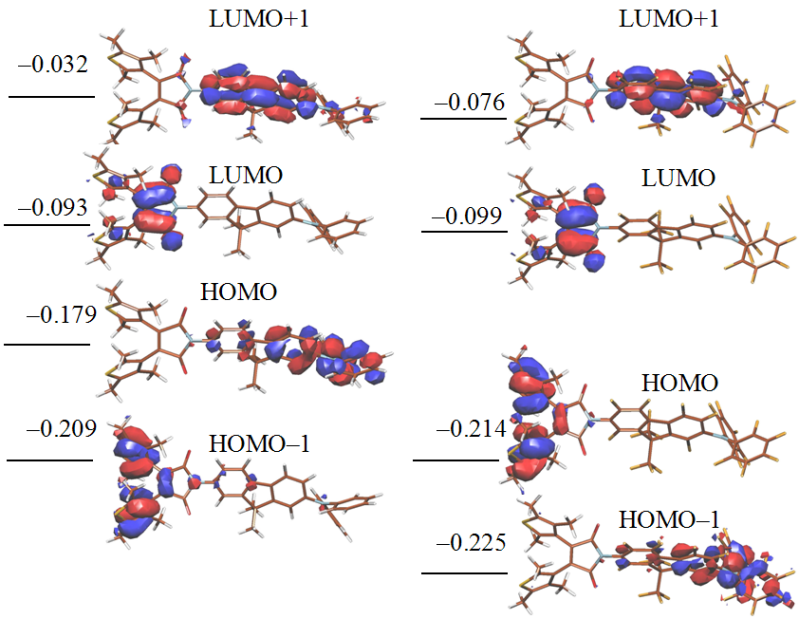

Figure 11. Kohn-Sham energy levels (a.u.) and orbital plots for open forms of the compounds 2b (left) and 2c (right) at the M05-2X/6-31G level of theory. While the orbitals essential for the ring closure are HOMO–1 and LUMO in 2b, they are HOMO and LUMO in 2c. This is the reason why the lowest excited state of 2c is photoreactive.

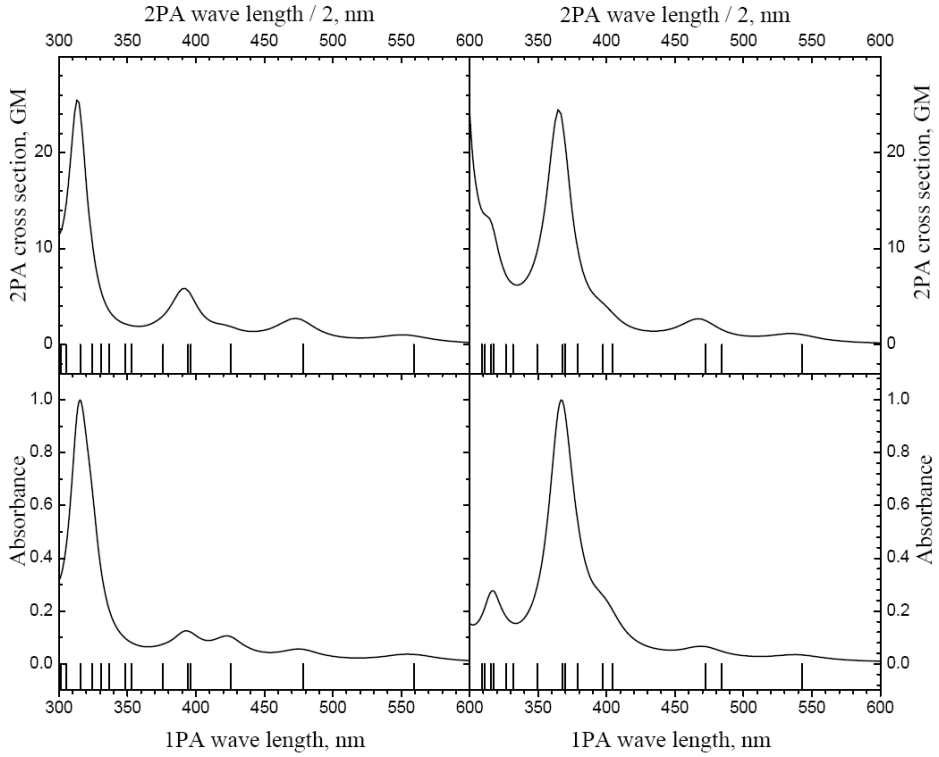

Figure 12. 1PA (bottom row) and 2PA (top row) spectra for molecules 2b (right column) and 2c (left column) calculated at the ATDA-B3LYP/6-31G//AM1 level of theory. Vertical lines correspond to calculated energies of excited states.

The theoretically predicted 1PA and 2PA spectra for the open form of molecules **2b** and **2c** are plotted in Figure 12. Both molecules demonstrate moderate 2PA cross-sections (ca. 30 GM) in the range of excitation energy 300 – 600 nm. To increase the 2PA cross-section some additional chemical modifications are necessary. This can be a subject of future studies.

4. Conclusions

We reviewed the current state of DFT-based methods developed for prediction of 2PA cross-sections and potential energy surfaces of the excited states. A recently proposed ATDA-DFT approach, based on the approximate second order response within density functional theory was shown to be capable to accomplish both goals. Apart from the quantitative

accuracy, this approach allows for qualitative interpretation of the electronic structure that leads to a better understanding of the photophysical and photochemical processes involved. ATDA-DFT approach (*a posteriori* Tamm-Dancoff approximation) accounts for both single and double excitations appearing in the first and second order time-dependent DFT in the Coupled Electronic Oscillator formalism. The permanent and transition dipole moments, calculated at this approximation, reproduce well high-level *ab initio* values, and ATDA predicted 2PA cross-sections are in agreement with the third-order TD-DFT results. Smooth potential energy surfaces were obtained by replacing the ground state energy component of the excited state with the one obtained in the unrestricted broken symmetry Kohn-Sham formalism (termed here ATDA-UDFT). The importance of excited state geometry optimization (as opposed to the habitual use of unrelaxed ground state geometries) in accurate prediction of these potential energy surfaces was confirmed. For the lack of analytical derivatives at the ATDA-UDFT theory level the lowest single and double excited state geometry is approximated using the Slater Transition State method (STS-DFT). The combined ATDA-UDFT//STS-DFT approach was shown to somewhat underestimate energies of the both excited states but closely reproduce the state ordering and the energy crossovers predicted at high-level multireference perturbation theory level for the prototypical hexatriene/cyclohexadiene system. The approach was also able to explain the experimentally observed slow photochemical cycloreversion rates in model dithioarylethenes.

The ATDA-UDFT//STS-DFT approach was also used to explain the loss of photochromic reactivity in the prototype two-photon absorbing photoswitch. The nature of the loss was traced to the presence of a barrier on the potential energy surface of the lowest excited state. The Kohn-Sham orbital analysis revealed this barrier to be the result of the lone pair orbital of the donor chromophore group appearing inside the HOMO-LUMO gap of the essential orbitals in the photoswitching molecular core, so that the lowest excited state changed from the photoreactive type to the charge transfer type. In order to restore the photoreactivity the stabilization of the lone pair orbital to the energy below the HOMO-LUMO gap was suggested by means of perfluorination of the two-photon absorbing chromophore pendant group. This substitution was found to restore the order of the essential orbitals and eliminate the energy barrier on the excited state potential surface. Based on these findings, the design principle for the new photochromic molecules was formulated: substituents should not introduce any electron energy levels within the HOMO-LUMO gap between essential orbitals of the photoreactive fragment. This principle will assist in future development of the materials for three-dimensional optical data storage devices with unprecedented storage capacity for advanced applications in Information Technology.

The ATDA-DFT approach was also found to predict state-to-state transition dipoles and permanent excited state dipoles accurately, as compared to the correlated wavefunction results. The two-photon absorption cross sections predictions were also accurate, as compared to the experimental data for a benchmark set. Thus, ATDA-DFT provides a tool that may be used in design of more efficient two-photon absorbing chromophores. The methods reviewed here are capable to accurately describe both nonlinear optical and photochemical properties of the material; they call for broader application and further development.

Acknowledgements

This work is supported in part by the National Science Foundation (CCF 0740344). Research was performed in part using (1) Stokes HPCC facility at UCF Institute for Simulation and Training (IST), (2) Bethe SMP server at UCF NanoScience Technology Center (NSTC), and (3) the National Energy Research Scientific Computing Center (NERSC) a DOE Office of Science user facility at Lawrence Berkely National Laboratory. AEM acknowledges ACS COMP Hewlett-Packard Outstanding Junior Faculty Award presented for this work at the Fall 2008 Annual Meeting of the American Chemical Society.

References

[1]. Kaneko, M. *MRS Bull.* **2006**, *31*, 314-317.
[2]. Wang, J. G.; Sun, C. J.; Hashimoto, Y.; Kono, J.; Khodaparast, G. A.; Cywinski, L.; Sham, L. J.; Sanders, G. D.; Stanton, C. J.; Munekata, H. *J. Phys.: Condens. Matter* **2006**, *18*, R501-R530.
[3]. Zhou, G. F. *Mater. Sci. Eng., A* **2001**, *304*, 73-80.
[4]. Kawata, S.; Kawata, Y. *Chem. Rev.* **2000**, *100*, 1777-1788.
[5]. Irie, M. *Chem. Rev.* **2000**, *100*, 1685-1716.
[6]. Parthenopoulos, D. A.; Rentzepis, P. M. *Science* **1989**, *245*, 843-845.
[7]. Saita, S.; Yamaguchi, T.; Kawai, T.; Irie, M. *Chem. Phys. Chem.* **2005**, *6*, 2300-2306.
[8]. Shipway, A. N.; Greenwald, M.; Jaber, N.; Litwak, A. M.; Reisman, B. J. *Jpn. J. Appl. Phys., Part 1* **2006**, *45*, 1229-1234.
[9]. Boggio-Pasqua, M.; Ravaglia, M.; Bearpark, M. J.; Garavelli, M.; Robb, M. A. *J. Phys. Chem. A* **2003**, *107*, 11139-11152.
[10]. Koppel, H.; Doscher, M.; Mahapatra, S. *Int. J. Quantum Chem* **2000**, *80*, 942-949.
[11]. Kendrick, B. K. *J. Chem. Phys.* **2001**, *114*, 8796-8819.
[12]. Hack, M. D.; Jasper, A. W.; Volobuev, Y. L.; Schwenke, D. W.; Truhlar, D. G. *J. Phys. Chem. A* **2000**, *104*, 217-232.
[13]. Jasper, A. W.; Truhlar, D. G. *J. Chem. Phys.* **2005**, *122*, 044101-16.
[14]. Vallet, V.; Lan, Z. G.; Mahapatra, S.; Sobolewski, A. L.; Domcke, W. *Faraday Discuss.* **2004**, *127*, 283-293.
[15]. Garavelli, M. *Theor. Chem. Acc.* **2006**, *116*, 87-105.
[16]. Truhlar, D. G.; Gordon, M. S. *Science* **1990**, *249*, 491-498.
[17]. Fuss, W.; Hering, P.; Kompa, K. L.; Lochbrunner, S.; Schikarski, T.; Schmid, W. E.; Trushin, S. A. *Ber. Bunsen-Ges. Phys. Chem* **1997**, *101*, 500-509.
[18]. Bernardi, F.; Olivucci, M.; Robb, M. A. *Chem. Soc. Rev.* **1996**, *25*, 321-328.
[19]. Fuss, W.; Lochbrunner, S.; Muller, A. M.; Schikarski, T.; Schmid, W. E.; Trushin, S. A. *Chem. Phys.* **1998**, *232*, 161-174.
[20]. Robb, M. A.; Garavelli, M.; Olivucci, M.; Bernardi, F. *Rev. Comput. Chem.* 2000; Vol. 15, p 87-146.
[21]. Toniolo, A.; Ben-Nun, M.; Martinez, T. J. *J. Phys. Chem. A* **2002**, *106*, 4679-4689.
[22]. Yarkony, D. R. *Faraday Discuss.* **2004**, *127*, 325-336.
[23]. Gilbert, A. T. B.; Besley, N. A.; Gill, P. M. W. *J. Phys. Chem. A* **2008**, *112*, 13164-13171.
[24]. Frank, I.; Hutter, J.; Marx, D.; Parrinello, M. *J. Chem. Phys.* **1998**, *108*, 4060-4069.
[25]. Ziegler, T.; Rauk, A.; Baerends, E. J. *Theor. Chim. Acta* **1977**, *43*, 261-271.
[26]. Billeter, S. R.; Egli, D. *J. Chem. Phys.* **2006**, *125*, 224103(18).
[27]. Doltsinis, N. L.; Marx, D. *Phys. Rev. Lett.* **2002**, *88*, 166402-4.
[28]. Runge, E.; Gross, E. K. U. *Phys. Rev. Lett.* **1984**, *52*, 997-1000.
[29]. Levine, B. G.; Ko, C.; Quenneville, J.; Martinez, T. J. *Mol. Phys.* **2006**, *104*, 1039-1051.
[30]. Mikhailov, I. A.; Belfield, K. D.; Masunov, A. E. *J. Phys. Chem. A* **2009**, *113*, 7080-7089.
[31]. Kohn, W.; Sham, L. J. *Phys. Rev.* **1965**, *140*, A1133-A1138.
[32]. Adamo, C.; di Matteo, A.; Barone, V. *Adv. Quantum Chem.* **2000**, *36*, 45-75.
[33]. Gritsenko, O. V.; Baerends, E. J. *Theor. Chem. Acc.* **1997**, *96*, 44-50.
[34]. Takeda, R.; Yamanaka, S.; Yamaguchi, K. *Int. J. Quantum Chem* **2005**, *101*, 658-665.
[35]. Becke, A. D. *J. Chem. Phys.* **1997**, *107*, 8554-8560.
[36]. Grimme, S.; Waletzke, M. *J. Chem. Phys.* **1999**, *111*, 5645-5655.
[37]. Gimme, S. *J. Chem. Phys.* **2006**, *124*, 034108(16).
[38]. Yamanaka, S.; Nakata, K.; Takada, T.; Kusakabe, K.; Ugaide, J. M.; Yamaguchi, K. *Chem. Lett.* **2006**, *35*, 242-247.
[39]. Gutle, C.; Savin, A. *Phys. Rev. A: At. Mol. Opt. Phys.* **2007**, *75*, 032519-17.
[40]. Langhoff, P. W.; Epstein, S. T.; Karplus, M. *Rev. Mod. Phys.* **1972**, *44*, 602-644.
[41]. Hansen, A. E.; Bouman, T. D. *Mol. Phys.* **1979**, *37*, 1713-1724.
[42]. Casida, M. E. *Recent Advances in Density-Functional Methods*; Chong, D. A., Ed. 1995; Vol. 3 of Part I.
[43]. Stratmann, R. E.; Scuseria, G. E.; Frisch, M. J. *J. Chem. Phys.* **1998**, *109*, 8218-8224.
[44]. Dunning, T. H.; McKoy, V. *J. Chem. Phys.* **1967**, *47*, 1735-1747.
[45]. Hirata, S.; Head-Gordon, M. *Chem. Phys. Lett.* **1999**, *314*, 291-299.
[46]. Savin, A.; Umrigar, C. J.; Gonze, X. *Chem. Phys. Lett.* **1998**, *288*, 391-395.

[47]. Neugebauer, J.; Baerends, E. J.; Nooijen, M. *J. Chem. Phys.* **2004**, *121*, 6155-6166.
[48]. Hsu, C. P.; Hirata, S.; Head-Gordon, M. *J. Phys. Chem. A* **2001**, *105*, 451-458.
[49]. Hirata, S.; Head-Gordon, M. *Chem. Phys. Lett.* **1999**, *302*, 375-382.
[50]. Catalan, J.; de Paz, J. L. G. *J. Chem. Phys.* **2004**, *120*, 1864-1872.
[51]. Starcke, J. H.; Wormit, M.; Schirmer, J.; Dreuw, A. *Chem. Phys.* **2006**, *329*, 39-49.
[52]. Wanko, M.; Garavelli, M.; Bernardi, F.; Niehaus, T. A.; Frauenheim, T.; Elstner, M. *J. Chem. Phys.* **2004**, *120*, 1674-1692.
[53]. Fantacci, S.; Migani, A.; Olivucci, M. *J. Phys. Chem. A* **2004**, *108*, 1208-1213.
[54]. Shao, Y. H.; Head-Gordon, M.; Krylov, A. I. *J. Chem. Phys.* **2003**, *118*, 4807-4818.
[55]. Guan, J. G.; Wang, F.; Ziegler, T.; Cox, H. *J. Chem. Phys.* **2006**, *125*, 044314(9).
[56]. Maitra, N. T.; Zhang, F.; Cave, R. J.; Burke, K. *J. Chem. Phys.* **2004**, *120*, 5932-5937.
[57]. Shibuya, T.; Rose, J.; McKoy, V. *J. Chem. Phys.* **1973**, *58*, 500-507.
[58]. Jorgensen, P.; Swanstrom, P.; Yeager, D. L.; Olsen, J. *Int. J. Quantum Chem* **1983**, *23*, 959-971.
[59]. Hirata, S.; Nooijen, M.; Grabowski, I.; Bartlett, R. J. *J. Chem. Phys.* **2001**, *114*, 3919-3928.
[60]. Stanton, J. F.; Bartlett, R. J. *J. Chem. Phys.* **1993**, *98*, 7029-7039.
[61]. DelBene, J. E.; Watts, J. D.; Bartlett, R. J. *J. Chem. Phys.* **1997**, *106*, 6051-6060.
[62]. Dalgaard, E. *J. Chem. Phys.* **1980**, *72*, 816-823.
[63]. Olsen, J.; Jorgensen, P. *J. Chem. Phys.* **1985**, *82*, 3235-3264.
[64]. Vahtras, O.; Agren, H.; Jorgensen, P.; Jorgen, H.; Jensen, A.; Helgaker, T.; Olsen, J. *J. Chem. Phys.* **1992**, *97*, 9178-9187.
[65]. Sasagane, K.; Aiga, F.; Itoh, R. *J. Chem. Phys.* **1993**, *99*, 3738-3778.
[66]. Luo, Y.; Agren, H.; Stafstrom, S. *J. Phys. Chem.* **1994**, *98*, 7782-7789.
[67]. Salek, P.; Vahtras, O.; Guo, J. D.; Luo, Y.; Helgaker, T.; Agren, H. *Chem. Phys. Lett.* **2003**, *374*, 446-452.
[68]. Dalgaard, E.; Monkhorst, H. J. *Phys. Rev. A: At. Mol. Opt. Phys.* **1983**, *28*, 1217-1222.
[69]. Larsen, H.; Jorgensen, P.; Olsen, J.; Helgaker, T. *J. Chem. Phys.* **2000**, *113*, 8908-8917.
[70]. Furche, F. *J. Chem. Phys.* **2001**, *114*, 5982-5992.
[71]. Salek, P.; Vahtras, O.; Helgaker, T.; Agren, H. *J. Chem. Phys.* **2002**, *117*, 9630-9645.
[72]. Cronstrand, P.; Luo, Y.; Agren, H. *Adv. Quantum Chem.* **2005**, *50*, 1-21.
[73]. Knoester, J.; Mukamel, S. *Phys. Rev. A: At. Mol. Opt. Phys.* **1989**, *39*, 1899-1914.
[74]. Tretiak, S.; Mukamel, S. *Chem. Rev.* **2002**, *102*, 3171-3212.
[75]. Tretiak, S.; Chernyak, V. *J. Chem. Phys.* **2003**, *119*, 8809-8823.
[76]. Ziegler, T.; Seth, M.; Krykunov, M.; Autschbach, J.; Wang, F. *The Journal of Chemical Physics* **2009**, *130*, 154102-8.
[77]. Ziegler, T.; Seth, M.; Krykunov, M.; Autschbach, J.; Wang, F. *Journal of Molecular Structure: Theochem* **2009**, *914*, 106-109.
[78]. Katz, H. E. *Chem. Mater.* **2004**, *16*, 4748-4756.
[79]. Dalton, L. R. *J. Phys.: Condens. Matter* **2003**, *15*, R897-R934.
[80]. Perry, J. W.; Marder, S. R.; Meyers, F.; Lu, D.; Chen, G.; Goddard, W. A.; Bredas, J. L.; Pierce, B. M. *Polymers for Second-Order Nonlinear Optics,*; American Chemical Society: Washington, DC, **1995**, *601*, 45-56.
[81]. Suponitsky, K. Y.; Timofeeva, T. V.; Antipin, M. Y. *Usp. Khim.* **2006**, *75*, 515-556.
[82]. Schulten, K.; Karplus, M. *Chem. Phys. Lett.* **1972**, *14*, 305-309.
[83]. Olchawa, R. *Phys. B (Amsterdam, Neth.)* **2000**, *291*, 29-33.
[84]. Barford, W.; Bursill, R. J.; Lavrentiev, M. Y. *Phys. Rev. B: Condens. Matter* **2001**, *63*, 195108-8.
[85]. Orr, B. J.; Ward, J. F. *Mol. Phys.* **1971**, *20*, 513-526.
[86]. Wu, J. W.; Heflin, J. R.; Norwood, R. A.; Wong, K. Y.; Zamanikhamiri, O.; Garito, A. F.; Kalyanaraman, P.; Sounik, J. *J. Opt. Soc. Am. B: Opt. Phys.* **1989**, *6*, 707-720.
[87]. McWilliams, P. C. M.; Hayden, G. W.; Soos, Z. G. *Phys. Rev. B: Condens. Matter* **1991**, *43*, 9777-9791.
[88]. Guo, D.; Mazumdar, S.; Dixit, S. N.; Kajzar, F.; Jarka, F.; Kawabe, Y.; Peyghambarian, N. *Phys. Rev. B: Condens. Matter* **1993**, *48*, 1433-1459.
[89]. Fitch, W. L.; McGregor, M.; Katritzky, A. R.; Lomaka, A.; Petrukhin, R.; Karelson, M. *J. Chem. Inf. Comput. Sci.* **2002**, *42*, 830-840.
[90]. Rumi, M.; Ehrlich, J. E.; Heikal, A. A.; Perry, J. W.; Barlow, S.; Hu, Z. Y.; McCord-Maughon, D.; Parker, T. C.; Rockel, H.; Thayumanavan, S.; Marder, S. R.; Beljonne, D.; Bredas, J. L. *J. Am. Chem. Soc.* **2000**, *122*, 9500-9510.
[91]. Beljonne, D.; Shuai, Z.; SerranoAndres, L.; Bredas, J. L. *Chem. Phys. Lett.* **1997**, *279*, 1-8.
[92]. Mikhailov, I. A.; Tafur, S.; Masunov, A. E. *Phys. Rev. A: At. Mol. Opt. Phys.* **2008**, *77*, 012510-11.
[93]. Hashimoto, T.; Nakano, H.; Hirao, K. *J. Chem. Phys.* **1996**, *104*, 6244-6258.
[94]. Pariser, R. *J. Chem. Phys.* **1956**, *24*, 250-268.
[95]. Hirao, K.; Nakano, H.; Nakayama, K.; Dupuis, M. *J. Chem. Phys.* **1996**, *105*, 9227-9239.
[96]. Malrieu, J. P.; Nebotgil, I.; Sanchezmarin, J. *Pure Appl. Chem.* **1984**, *56*, 1241-1254.
[97]. Glushkov, V. N. *Opt. Spectrosc.* **2005**, *99*, 684-689.
[98]. Löwdin, P.-O.; Shull, H. *Phys. Rev.* **1956**, *101*, 1730.
[99]. Headgordon, M.; Rico, R. J.; Oumi, M.; Lee, T. J. *Chem. Phys. Lett.* **1994**, *219*, 21-29.
[100]. Kurashige, Y.; Nakano, H.; Nakao, Y.; Hirao, K. *Chem. Phys. Lett.* **2004**, *400*, 425-429.
[101]. Sekino, H.; Bartlett, R. J. *Adv. Quantum Chem.* **1999**, *35*, 149-173.
[102]. Nakatsuji, H. *Chem. Phys. Lett.* **1991**, *177*, 331-337.
[103]. Saha, B.; Ehara, M.; Nakatsuji, H. *J. Chem. Phys.* **2006**, *125*, 014316-14.
[104]. Kitao, O.; Nakatsuji, H. *Chem. Phys. Lett.* **1988**, *143*, 528-534.
[105]. Ostojic, B.; Domcke, W. *Chem. Phys.* **2001**, *269*, 1-10.
[106]. Kawski, A.; Kuklinski, B.; Bojarski, P. *Chem. Phys.* **2006**, *330*, 307-312.
[107]. Bublitz, G. U.; Boxer, S. G. *Annu. Rev. Phys. Chem.* **1997**, *48*, 213-242.
[108]. Korter, T. M.; Borst, D. R.; Butler, C. J.; Pratt, D. W. *J. Am. Chem. Soc.* **2001**, *123*, 96-99.
[109]. Nakayama, K.; Nakano, H.; Hirao, K. *Int. J. Quantum Chem* **1998**, *66*, 157-175.
[110]. Dunning, T. H. *J. Chem. Phys.* **1989**, *90*, 1007-1023.
[111]. Stanton, J. F.; Gauss, J.; Watts, J. D.; Lauderdale, W. J.; Bartlett, R. J.; Quantum Theory Project; Departments of Chemistry and Physics, University of Florida: Gainesville FL, 1993.
[112]. Frisch, M. J.; Trucks, G. W.; Schlegel, H. B.; Scuseria, G. E.; Robb, M. A.; Cheeseman, J. R.; Montgomery, J., J. A. ; Vreven, T.; Kudin, K. N.; Burant, J. C.; Millam, J. M.; Iyengar, S. S.; Tomasi, J.; Barone, V.; Mennucci, B.; Cossi, M.; Scalmani, G.; Rega, N.; Petersson, G. A.; Nakatsuji, H.; Hada, M.; Ehara, M.; Toyota, K.; Fukuda, R.; Hasegawa, J.; Ishida, M.; Nakajima, T.; Honda, Y.; Kitao, O.; Nakai, H.; Klene, M.; Li, X.; Knox, J. E.; Hratchian, H. P.; Cross, J. B.; Bakken, V.; Adamo, C.; Jaramillo, J.; Gomperts, R.; Stratmann, R. E.; Yazyev, O.; Austin, A. J.; Cammi, R.; Pomelli, C.; Ochterski, J. W.; Ayala, P. Y.; Morokuma, K.; Voth, G. A.; Salvador, P.; Dannenberg, J. J.; Zakrzewski, V. G.; Dapprich, S.; Daniels, A. D.; Strain, M. C.; Farkas, O.; Malick, D. K.; Rabuck, A. D.; Raghavachari, K.; Foresman, J. B.; Ortiz, J. V.; Cui, Q.; Baboul, A. G.; Clifford, S.; Cioslowski, J.; Stefanov, B. B.; Liu, G.; Liashenko, A.; Piskorz, P.; Komaromi, I.; Martin, R. L.; Fox, D. J.; Keith, T.; Al-Laham, M. A.; Peng, C. Y.; Nanayakkara, A.; Challacombe, M.; Gill, P. M. W.; Johnson, B.; Chen, W.; Wong, M. W.; Gonzalez, C.; Pople, J. A.; Revision E.1 ed.; Gaussian, Inc.: Wallingford CT, 2004.
[113]. Frisch, M. J.; Trucks, G. W.; Schlegel, H. B.; Scuseria, G. E.; Robb, M. A.; Cheeseman, J. R.; Montgomery, J., J. A. ; Vreven, T.; Kudin, K. N.; Burant, J. C.; Millam, J. M.; Iyengar, S. S.; Tomasi, J.; Barone, V.; Mennucci, B.; Cossi, M.; Scalmani, G.; Rega, N.; Petersson, G. A.; Nakatsuji, H.; Hada, M.; Ehara, M.; Toyota, K.; Fukuda, R.; Hasegawa, J.; Ishida, M.; Nakajima, T.; Honda, Y.; Kitao, O.; Nakai, H.; Klene, M.; Li, X.; Knox, J. E.; Hratchian, H. P.; Cross, J. B.; Bakken, V.; Adamo, C.; Jaramillo, J.; Gomperts, R.; Stratmann, R. E.; Yazyev, O.; Austin, A. J.; Cammi, R.; Pomelli, C.; Ochterski, J. W.; Ayala, P. Y.; Morokuma, K.; Voth, G. A.; Salvador, P.; Dannenberg, J. J.; Zakrzewski, V. G.; Dapprich, S.; Daniels, A. D.; Strain, M. C.; Farkas, O.; Malick, D. K.; Rabuck, A. D.; Raghavachari, K.; Foresman, J. B.; Ortiz, J. V.; Cui, Q.; Baboul, A. G.; Clifford, S.; Cioslowski, J.; Stefanov, B. B.; Liu, G.; Liashenko, A.; Piskorz, P.; Komaromi, I.; Martin, R. L.; Fox, D. J.; Keith, T.; Al-Laham, M. A.; Peng, C. Y.; Nanayakkara, A.; Challacombe, M.; Gill, P. M. W.; Johnson, B.; Chen, W.; Wong, M. W.; Gonzalez, C.; Pople, J. A.; Revision A.11 ed.; Gaussian, Inc.: Pittsburgh PA, 1998.
[114]. Cumpston, B. H.; Ananthavel, S. P.; Barlow, S.; Dyer, D. L.; Ehrlich, J. E.; Erskine, L. L.; Heikal, A. A.; Kuebler, S. M.; Lee, I. Y. S.; McCord-Maughon, D.; Qin, J. Q.; Rockel, H.; Rumi, M.; Wu, X. L.; Marder, S. R.; Perry, J. W. *Nature* **1999**, *398*, 51-54.
[115]. Kagotani, Y.; Miyajima, K.; Oohata, G.; Saito, S.; Ashida, M.; Edamatsu, K.; Itoh, T. *J. Lumin.* **2005**, *112*, 113-116.
[116]. Zipfel, W. R.; Williams, R. M.; Christie, R.; Nikitin, A. Y.; Hyman, B. T.; Webb, W. W. In *National Academy of Sciences of the United States of America* **2003**, *100*, 7075-7080.
[117]. Wang, C. K.; Macak, P.; Luo, Y.; Agren, H. *J. Chem. Phys.* **2001**, *114*, 9813-9820.
[118]. Albota, M.; Beljonne, D.; Bredas, J. L.; Ehrlich, J. E.; Fu, J. Y.; Heikal, A. A.; Hess, S. E.; Kogej, T.; Levin, M. D.; Marder, S. R.; McCord-Maughon, D.; Perry, J. W.; Rockel, H.; Rumi, M.; Subramaniam, C.; Webb, W. W.; Wu, X. L.; Xu, C. *Science* **1998**, *281*, 1653-1656.
[119]. Belfield, K. D.; Schafer, K. J.; Liu, Y. U.; Liu, J.; Ren, X. B.; Van Stryland, E. W. *J. Phys. Org. Chem.* **2000**, *13*, 837-849.
[120]. Belfield, K. D.; Morales, A. R.; Kang, B. S.; Hales, J. M.; Hagan, D. J.; Van Stryland, E. W.; Chapela, V. M.; Percino, J. *Chem. Mater.* **2004**, *16*, 4634-4641.
[121]. Kim, S.; Wang, Z.; Hagan, D. J.; Van Stryland, E. W.; Kobyakov, A.; Lederer, F.; Assanto, G. *IEEE J. Quantum Electron.* **1998**, *34*, 666-672.
[122]. Ventelon, L.; Moreaux, L.; Mertz, J.; Blanchard-Desce, M. *Chem. Commun.* **1999**, 2055-2056.
[123]. Kim, O. K.; Lee, K. S.; Woo, H. Y.; Kim, K. S.; He, G. S.; Swiatkiewicz, J.; Prasad, P. N. *Chem. Mater.* **2000**, *12*, 284-+.
[124]. Mikhailov, I. A.; Bondar, M. V.; Belfield, K. D.; Masunov, A. E. *J. Phys. Chem. C* **2009**, *113*, 20719-20724.

[125]. Suponitsky, K. Y.; Masunov, A. E.; Antipin, M. Y. *Mendeleev Commun.* **2009**, *19*, 311-313.
[126]. Iordanov, T. D.; Davis, J. L.; Masunov, A. E.; Levenson, A.; Przhonska, O. V.; Kachkovski, A. D. *Int. J. Quantum Chem* **2009**, *109*, 3592-3601.
[127]. Suponitsky, K. Y.; Liao, Y.; Masunov, A. E. *J. Phys. Chem. A* **2009**, *113*, 10994-11001.
[128]. Toro, C.; De Boni, L.; Yao, S.; Ritchie, J. P.; Masunov, A. E.; Belfield, K. D.; Hernandez, F. E. *J. Chem. Phys.* **2009**, *130*, 6.
[129]. Belfield, K. D.; Bondar, M. V.; Hernandez, F. E.; Masunov, A. E.; Mikhailov, I. A.; Morales, A. R.; Przhonska, O. V.; Yao, S. *J. Phys. Chem. C* **2009**, *113*, 4706-4711.
[130]. Suponitsky, K. Y.; Masunov, A. E.; Antipin, M. Y. *Mendeleev Commun.* **2008**, *18*, 265-267.
[131]. Suponitsky, K. Y.; Tafur, S.; Masunov, A. E. *J. Chem. Phys.* **2008**, *129*, 11.
[132]. Toro, C.; Thibert, A.; De Boni, L.; Masunov, A. E.; Hernandez, F. E. *J. Phys. Chem. B* **2008**, *112*, 929-937.
[133]. Kauffman, J. F.; Turner, J. M.; Alabugin, I. V.; Breiner, B.; Kovalenko, S. V.; Badaeva, E. A.; Masunov, A.; Tretiak, S. *J. Phys. Chem. A* **2006**, *110*, 241-251.
[134]. Masunov, A.; Tretiak, S.; Hong, J. W.; Liu, B.; Bazan, G. C. *J. Chem. Phys.* **2005**, *122*, 10.
[135]. Kobko, N.; Masunov, A.; Tretiak, S. *Chem. Phys. Lett.* **2004**, *392*, 444-451.
[136]. Fabian, J.; Diaz, L. A.; Seifert, G.; Niehaus, T. *J. Mol. Struct.* **2002**, *594*, 41-53.
[137]. Hales, J. M.; Hagan, D. J.; Van Stryland, E. W.; Schafer, K. J.; Morales, A. R.; Belfield, K. D.; Pacher, P.; Kwon, O.; Zojer, E.; Bredas, J. L. *J. Chem. Phys.* **2004**, *121*, 3152-3160.
[138]. Tafur, S.; Mikhailov, I.; Belfield, K.; Masunov, A. *Computational Science – LNCS* **2009**, *5545*, 179-188.
[139]. Belfield, K. D.; Bondar, M. V.; Hales, J. M.; Morales, A. R.; Przhonska, O. V.; Schafer, K. J. *J. Fluoresc.* **2005**, *15*, 3-11.
[140]. Belfield, K. D.; Yao, S.; Morales, A. R.; Hales, J. M.; Hagan, D. J.; Van Stryland, E. W.; Chapela, V. M.; Percino, J. *Polym. Adv. Technol.* **2005**, *16*, 150-155.
[141]. Belfield, K. D.; Bondar, M. V.; Cohanoschi, I.; Hernandez, F. E.; Kachkovsky, O. D.; Przhonska, O. V.; Yao, S. *Appl. Opt.* **2005**, *44*, 7232-7238.
[142]. Schafer-Hales, K. J.; Belfield, K. D.; Yao, S.; Frederiksen, P. K.; Hales, J. M.; Kolattukudy, P. E. *J. Biomed. Opt.* **2005**, *10*.
[143]. Belfield, K. D.; Schafer, K. J. *Chem. Mater.* **2002**, *14*, 3656-3662.
[144]. Day, P. N.; Nguyen, K. A.; Pachter, R. *J. Phys. Chem. B* **2005**, *109*, 1803-1814.
[145]. Day, P. N.; Nguyen, K. A.; Pachter, R. *J. Chem. Phys.* **2006**, *125*, 094103(13).
[146]. Ohta, K.; Kamada, K. *J. Chem. Phys.* **2006**, *124*, 124303-11.
[147]. Cronstrand, P.; Jansik, B.; Jonsson, D.; Luo, Y.; Agren, H. *J. Chem. Phys.* **2004**, *121*, 9239-9246.
[148]. Masunov, A. M.; Tretiak, S. *J. Phys. Chem. B* **2004**, *108*, 899-907.
[149]. Martin, R. L. *J. Chem. Phys.* **2003**, *118*, 4775-4777.
[150]. Kokalj, A. *Comput. Mater. Sci.* **2003**, *28*, 155-168. Code available from http://www.xcrysden.org/
[151]. Belfield, K. D.; Bondar, M. V.; Hernandezt, F. E.; Przhonska, O. V.; Yao, S. *J. Phys. Chem. B* **2007**, *111*, 12723-12729.
[152]. Corredor, C. C. Ph. D. dissertation, University of Central Florida, 2007.
[153]. Gunnarsson, O.; Lundqvist, B. I. *Phys. Rev. B: Condens. Matter* **1976**, *13*, 4274-4298.
[154]. Savin, A.; Colonna, F.; Pollet, R. *Int. J. Quantum Chem* **2003**, *93*, 166-190.
[155]. Della Sala, F.; Gorling, A. *J. Chem. Phys.* **2003**, *118*, 10439-10454.
[156]. Moreira, I. D. R.; Costa, R.; Filatov, M.; Illas, F. *J. Chem. Theory Comput.* **2007**, *3*, 764-774.
[157]. Cai, Z. L.; Reimers, J. R. *J. Chem. Phys.* **2000**, *112*, 527-530.
[158]. Casida, M. E.; Ipatov, A. *Abstr Pap Am Chem S* **2006**, *231*, 1.
[159]. Cave, R. J.; Zhang, F.; Maitra, N. T.; Burke, K. *Chem. Phys. Lett.* **2004**, *389*, 39-42.
[160]. Mikhailov, I. A.; Masunov, A. E. *Computational Science - LNCS* **2009**, *5545*, 169-178.
[161]. Slater, J. C. *Adv. Quantum Chem.* 1972; Vol. 6, p 1-92.
[162]. Noodleman, L.; Baerends, E. J. *J. Am. Chem. Soc.* **1984**, *106*, 2316-2327.
[163]. Liberman, D. A. *Phys. Rev. B: Condens. Matter* **2000**, *62*, 6851-6853.
[164]. Hu, C. P.; Sugino, O. *J. Chem. Phys.* **2007**, *126*, 074112(10).
[165]. Zhao, Y.; Schultz, N. E.; Truhlar, D. G. *J. Chem. Theory Comput.* **2006**, *2*, 364-382.
[166]. Takahashi, O.; Sumita, M. *J. Mol. Struct.* **2005**, *731*, 173-175.
[167]. Schaftenaar, G.; Noordik, J. H. *J. Comput. Aided Mol. Des.* **2000**, *14*, 123-134.
[168]. Kuthirummal, N.; Rudakov, F. M.; Evans, C. L.; Weber, P. M. *J. Chem. Phys.* **2006**, *125*, 133307-8.
[169]. Lochbrunner, S.; Fuss, W.; Schmid, W. E.; Kompa, K. L. *J. Phys. Chem. A* **1998**, *102*, 9334-9344.
[170]. Woodward, R. B.; Hoffmann, R. *J. Am. Chem. Soc.* **1965**, *87*, 395-397.
[171]. Longuet-Higgins, H. C.; Abrahamson, E. W. *J. Am. Chem. Soc.* **1965**, *87*, 2045-2046.
[172]. Michl, J. *Molecular Photochemistry* **1972**, *4*, 287-314.
[173]. Celani, P.; Ottani, S.; Olivucci, M.; Bernardi, F.; Robb, M. A. *J. Am. Chem. Soc.* **1994**, *116*, 10141-10151.
[174]. Celani, P.; Bernardi, F.; Robb, M. A.; Olivucci, M. *J. Phys. Chem.* **1996**, *100*, 19364-19366.
[175]. Garavelli, M.; Celani, P.; Fato, M.; Bearpark, M. J.; Smith, B. R.; Olivucci, M.; Robb, M. A. *J. Phys. Chem. A* **1997**, *101*, 2023-2032.
[176]. Tamura, H.; Nanbu, S.; Nakamura, H.; Ishida, T. *Chem. Phys. Lett.* **2005**, *401*, 487-491.
[177]. Tamura, H.; Nanbu, S.; Ishida, T.; Nakamura, H. *The Journal of Chemical Physics* **2006**, *124*, 084313-13.
[178]. Guillaumont, D.; Kobayashi, T.; Kanda, K.; Miyasaka, H.; Uchida, K.; Kobatake, S.; Shibata, K.; Nakamura, S.; Irie, M. *J. Phys. Chem. A* **2002**, *106*, 7222-7227.
[179]. Lafond, C.; Lessarda, R. A.; Bolteb, M.; Petkov, I. In *Part of the SPIE Conference on Photopolymer Device Physics, Chemistry, and Applications IV.*; SPIE-The International Society for Optical Engineering, Vol. 3417: Québec, Canada, 1998, p 216-227.
[180]. Andrasik, S. J.; Belfield, K. D.; Bondar, M. V.; Hernandez, F. E.; Morales, A. R.; Przhonska, O. V.; Yao, S. *ChemPhysChem* **2007**, *8*, 399-404.
[181]. Adronov, A.; Frechet, J. M. J.; He, G. S.; Kim, K. S.; Chung, S. J.; Swiatkiewicz, J.; Prasad, P. N. *Chem. Mater.* **2000**, *12*, 2838-2841.